Limitations in PPARα-dependent mitochondrial programming restrain the differentiation of human stem cell-derived β cells

Anne C. Lietzke[1,2], Emily M. Walker[1*], Elizabeth Bealer[3*], Kelly Crumley[3*], Jessica King[3*], Ava M. Stendahl[1], Jie Zhu[1], Gemma L. Pearson[1], Elena Levi-D'Ancona[1,4], Belle Henry-Kanarek[1,4], Rebecca K. Davidson[1], Jin Li[1], Emma C. Reck[1], Yifei Wu[1], Manikanta Arnipalli[5], John Paul Pham[3], Lakshmi Mundada[6,7,8], Vaibhav Sidarala[1], Todd J. Herron[6,7,8], Maria M. Coronel[3], Subramaniam Pennathur[5,8,9], Jesper G.S. Madsen[10], Lonnie D. Shea[3], and Scott A. Soleimanpour[1,8,9#]

[1]Division of Metabolism, Endocrinology and Diabetes and Department of Internal Medicine, University of Michigan Medical School, Ann Arbor, Michigan, USA.

[2]Department of Pharmacology Graduate Program, University of Michigan Medical School, Ann Arbor, Michigan, USA.

[3]Department of Biomedical Engineering, University of Michigan School of Engineering, Ann Arbor, Michigan, USA.

[4]Immunology Graduate Program, University of Michigan Medical School, Ann Arbor, Michigan, USA.

[5]Division of Nephrology and Department of Internal Medicine, University of Michigan Medical School, Ann Arbor, Michigan, USA

[6]Frankel Cardiovascular Regeneration Core Laboratory University of Michigan, Ann Arbor, MI, USA

[7]Division of Cardiology and Department of Internal Medicine, University of Michigan Medical School, Ann Arbor, Michigan, USA

[8]Department of Molecular and Integrative Physiology, University of Michigan, Ann Arbor, Michigan, USA

[9]VA Ann Arbor Healthcare System, Ann Arbor, Michigan, USA.

[10]Department of Biochemistry and Molecular Biology, University of Southern Denmark, Odense, Denmark

*These authors contributed equally to this work.

[#]Corresponding Author. Scott A. Soleimanpour, MD, 1000 Wall Street, Brehm Tower Room 6329, Ann Arbor, MI 48105, USA. Phone: (734) 763-0528 E-mail: ssol@med.umich.edu

ABSTRACT

Pluripotent stem cell (SC)-derived islets offer hope as a renewable source for β cell replacement for type 1 diabetes (T1D), yet functional and metabolic immaturity may limit their long-term therapeutic potential. Here, we show that limitations in mitochondrial transcriptional programming impede the formation of SC-derived β (SC-β) cells. Utilizing transcriptomic profiling, assessments of chromatin accessibility, mitochondrial phenotyping, and lipidomics analyses, we observed that SC-β cells exhibit reduced oxidative and mitochondrial fatty acid metabolism compared to primary human islets that are related to limitations in key mitochondrial transcriptional networks. Surprisingly, we found that reductions in glucose-stimulated mitochondrial respiration in SC-islets were not associated with alterations in mitochondrial mass, structure, or genome integrity. In contrast, SC-islets show limited expression of targets of PPARα, which regulate mitochondrial programming, yet whose functions in β cell differentiation are unknown. Importantly, treatment with WY14643, a potent PPARα agonist, induced expression of mitochondrial targets, improved insulin secretion, and increased the formation of SC-β cells both *in vitro* and following transplantation. Thus, PPARα-dependent mitochondrial programming promotes the differentiation of SC-β cells and may be a promising target to improve β cell replacement efforts for T1D.

INTRODUCTION

All forms of diabetes are associated with reduced mass and function of pancreatic islet β-cells, rendering the body unable to produce sufficient insulin to meet metabolic needs[1]. Thus, replacement of insulin-producing β cells remains a primary goal for diabetes therapy. Pluripotent stem cell (SC)-derived islets, which consist of a heterogeneous mixture of β cells, other islet hormone cell types, as well as immature progenitors and polyhormonal cells, are a promising source for β cell replacement, as these cells could be generated at scale to meet the substantial needs for patients with type 1 diabetes[2,3] (T1D). Directed differentiation of stem cells towards the β cell lineage requires a relatively lengthy (~1 month), complex, multi-stage protocol, including sequential use of small molecules and growth factors, cellular enrichment approaches, and modulation of spatial environments, which support the progression of SCs to progenitor cell types and eventually towards islets[4–8]. Despite the many advances in SC-islet differentiation, these protocols produce a relatively lower frequency of insulin$^+$ β-like cells that are not fully functional *in vitro* and have limited glucose-stimulated insulin secretion (GSIS) compared to β cells within primary human islets.

Optimal mitochondrial function is essential to maintain GSIS, yet mitochondrial respiration is impaired in SC-islets and is of unclear etiology[5,6,9,10]. Limitations in mitochondrial metabolism of SC-islets also persist following transplantation *in vivo*[6,10,11,12]. Further, several key aspects of mitochondrial metabolism in SC-islets, such as mitochondrial fatty acid metabolism, remain unexplored. Mitochondria are vital to the function of metabolic tissues, yet recent studies position mitochondria as more than client organelles tasked with energy production and have also been shown to regulate cell fate[13,14]. However, whether mitochondrial programming can promote the SC-derived β (SC-β) cell lineage is unknown.

Here, we hypothesized and tested how targeting mitochondrial programming would improve the differentiation and function of SC-β cells. The objectives of our studies were to carefully dissect the mitochondrial metabolic function of SC-β cells, interrogate mitochondrial

73 programming across β cell differentiation, and explore potential mitochondrial programming
74 pathways that could be targeted to enhance mitochondrial function and, ultimately, SC-β
75 differentiation. Together, we speculated our studies would mechanistically reveal how limitations
76 in mitochondrial metabolism serve as an impediment to optimal SC-β cell differentiation.
77

78 **RESULTS**

79 **SC-islets are transcriptionally and metabolically immature**

80 We generated SC-islets via directed differentiation of the H1 human embryonic stem (hES) cell
81 line towards a β cell fate utilizing a protocol developed by the Millman laboratory[4] (Fig. 1A and
82 S1A). To evaluate changes in transcriptional signatures throughout differentiation, as well as
83 markers of islet maturity, we performed RNA-sequencing (RNA-seq) across all differentiation
84 stages with comparison to human islet preparations from non-diabetic donors (Fig. S1B-E). These
85 studies, as well as immunofluorescence and flow cytometry studies, demonstrated that SCs, and
86 ultimately SC-islets, behaved largely as expected throughout differentiation, with expression of
87 stage-specific markers and expression of islet-specific hormones in stage 6 (as well as
88 polyhormonal cells; Fig. 1B-C and S1A). SC-islets also exhibited reduced expression of islet
89 hormones, with exception of *GHRL*, lower levels of β and α cell maturation markers, relative
90 hyporesponsiveness of insulin release to glucose- and KCl-stimulation, and lower insulin content
91 compared to primary human islets (Fig. 1D-F).

92 To complement our findings of transcriptional and functional immaturity in SC-islets, we
93 next profiled metabolic endpoints in SC-islets. We first surveyed the glycolytic intermediates
94 pyruvate and lactate by LC-MS, given the high importance of pyruvate utilization in mature β
95 cells[15–18]. We found that stage 5 and stage 6 cells increased pyruvate concentrations in response
96 to glucose stimulation, albeit at lower levels than human islets (Fig. 1G). Moreover, SCs at every
97 stage generated significantly higher quantities of lactate, including in stage 6 cells, as compared
98 to human islets (Fig. 1H). The presence of higher quantities of lactate in SC-islets than human

99 islets could be consistent with previous observations of defects in glycolytic flux, an inability to
100 silence lactate metabolism due to expression of disallowed genes (such as *LDHA*), or due to the
101 inability to switch from primarily glycolytic to oxidative metabolism in immature β cells, all of which
102 have been reported previously[5,6,10,18,19]. We next performed respirometry studies utilizing the
103 recently described Barofuse instrument, which allows for the assessment of respiration in a gas
104 pressure flow-based perifusion style platform[20]. We confirmed that SC-islets did not increase
105 oxygen consumption upon glucose stimulation as compared to human islets, which has been
106 shown previously[5,6,10] (Fig. 1I). We also observed that SC-islets displayed more sensitivity to the
107 effects of the ATP synthase inhibitor oligomycin, which is expected to lower oxygen consumption,
108 and the uncoupler FCCP, which transiently increases oxygen consumption, than primary human
109 islets, possibly suggesting that SC-islets may not be as uncoupled as primary human islets but
110 could also be related to relative differences in penetration of the compounds (Fig. 1I). Taken
111 together, SC-islets display a signature of transcriptional, functional, and metabolic immaturity.
112

113 **Mitochondrial DNA content, mass, and architecture in SC-islets are comparable to those**
114 **of human islets.**

115 Optimal β cell function is highly dependent on mitochondrial quality and health[21–23]. Given our
116 observations of transcriptional, functional, and metabolic immaturity in SC-islets, we profiled
117 mitochondrial mass and structure of SC-islets at different stages of differentiation and human
118 islets to obtain insights into limitations in mitochondrial respiration as recent studies have had
119 discordant results regarding reductions in mitochondrial mass in SC-islets compared to primary
120 human islets[5,10]. To survey mitochondrial genome integrity, we measured mitochondrial (mt)DNA
121 content, and while we found higher mtDNA content in stage 0 embryonic stem cells, we noted no
122 significant differences between stage 1-6 cells and human islets (Fig. 2A). To next determine if
123 there were deficiencies in mtDNA replication, we evaluated the initiation of first strand replication.
124 In mtDNA replication, first strand synthesis begins with formation of the D-loop. Elongation of the

125 7S sequence, which is contained in the D-loop, into the nearby region, *Cytb*, signifies committed
126 initiation of first strand replication. We assessed both D-loop formation and first strand replication
127 initiation and found no differences between stage 0-6 cells and human islets (Fig. 2B). We also
128 observed no differences in mitochondrial mass in stage 0-6 cells compared to human islets by
129 use of two complementary approaches; namely, citrate synthase activity and TOM20 protein
130 expression (Fig. 2C-D and S1F). To assess mitochondrial ultrastructure, we next performed
131 transmission electron microscopy. While we noted a lower frequency of mature insulin granules,
132 as previously described[5,6,24,25], we did not observe any differences in quantitative measures of
133 mitochondrial architecture in stage 6 SC-β cells compared to primary human β cells (Fig. 2E).
134 Together, these results suggest that limitations in mitochondrial respiration in SC-islets were not
135 a consequence of reduced mitochondrial genome integrity, DNA replication, mass, or structure.
136

137 **Transcriptomic profiling reveals potential limitations in mitochondrial metabolism in SC-**
138 **islets**

139 Due to the similarities in mitochondrial genome integrity, DNA replication, mass, and structure
140 between SC-islets and human islets, we next explored potential transcriptional differences that
141 might provide mechanistic insights into limitations in glucose-stimulated mitochondrial respiration
142 in SC-islets. Following a comparison of RNA-seq data between stage 6 SC-islets and human
143 islets, we found that 11,858 genes were significantly differentially expressed, including 405 genes
144 represented within MitoCarta 3.0[26], a curated set of nuclear and mitochondrial-encoded genes
145 with high confidence of localization to the mitochondria (Fig. 3A). While we observed dynamic
146 changes in expression of MitoCarta genes throughout differentiation, we noted a subset of highly
147 expressed MitoCarta genes in primary human islets that appeared to remain relatively lowly
148 expressed throughout SC differentiation, including by stage 6 (Fig. 3B). Pathways analysis of
149 differentially expressed MitoCarta genes showed differences in fatty acid metabolism, amino acid
150 metabolism, and oxidative phosphorylation (OXPHOS) (Fig. 3C-D). As there were a greater

151 number of downregulated Mitocarta 3.0 genes in SC-islets compared to human islets, we wanted
152 to understand the possible biological processes associated with these gene targets via the Search
153 Tool for Recurring Instances of Neighboring Genes (STRING) database[27]. Following STRING
154 analysis of significantly downregulated MitoCarta genes from stage 6 SC-islets, gene ontology
155 (GO) enrichment analysis was used to clarify pathways related to connections identified by
156 STRING. Pathways identified were related to mitochondrial translation, the electron transport
157 chain (ETC)-OXPHOS system, and lipid metabolism (Fig. 3E). Collectively, our transcriptomic
158 studies revealed several pathways that could contribute to limitations in mitochondrial metabolism
159 in SC-islets.
160
161 **Limitations in the OXPHOS machinery and mitochondrial lipid metabolism in SC-islets**
162 We next wished to clarify the specific nature of transcriptional defects affecting mitochondria in
163 SC-islets. An initial question was whether the limitations in SC-islet mitochondria were related to
164 an impairment in the shift of the glycolytic to OXPHOS metabolic program, which was previously
165 observed in human induced pluripotent stem cell (iPSC)-derived islets[11]. While we observed that
166 expression of genes related to glucose transport and glycolysis were enriched in stage 0
167 pluripotent cells, we did not observe differences in the glycolytic gene expression program
168 between stage 6 SC-islets and human islets (Fig. 4A). We also did not observe a significant
169 difference in the overall RNA expression of genes encoding the entirety of TCA cycle enzymes or
170 enzymes/transporters involved in lactate metabolism between stage 6 SC-islets and human islets,
171 whereas these genes were more highly enriched in stage 0 ES cells (Fig. S1G). We next
172 considered the possibility that mitochondrial impairments in SC-islets could be related to
173 limitations in the β cell OXPHOS machinery. Indeed, we observed a notable subset of 29
174 OXPHOS gene targets that were enriched in human islets compared to stage 6 SC-islets (Fig.
175 4B-C). These upregulated targets in human islets included genes encoding subunits of all 5 ETC
176 complexes, as well as complex assembly factors (Fig. 4B-C). Notably, stage 0 pluripotent cells

177 also had an enrichment of a subset of OXPHOS gene targets compared to stage 1-6 cells;
178 however, these genes appeared to be largely distinct from those upregulated within human islets
179 (Fig. 4B). To confirm that this phenotype was specific to SC-β cells compared to other SC-islet
180 cell types, we re-analyzed data from a recently published single-cell RNA-seq dataset comparing
181 SC-islets and human islets, as it has been observed that the various directed differentiation
182 protocols from independent laboratories produce SC-islets with similar transcriptomic profiles[28,29].
183 Indeed, we observed that >50% of OXPHOS gene targets were lower in SC-β cells compared to
184 primary human β cells, whereas there was no significant differences in glycolytic gene expression
185 between the groups (Fig. 4D). Reduced expression of OXPHOS genes appeared to be β cell-
186 specific, as we did not find robust differences in SC-α cells compared to primary human α cells
187 (Fig. 4D). Lower expression of ETC and OXPHOS gene targets in SC-β cells was also supported
188 by transcriptomic profiling by others[6]. We next measured expression of subunits of OXPHOS
189 complexes via Western blot and found that their expression was significantly lower in SCs
190 compared to human islets across all differentiation stages (Fig. 4E). Thus, we observed lower
191 expression of components of the OXPHOS machinery in SCs compared to human islets that
192 appear to be distinct from programming of the glycolytic gene network.

193 While β cells are not classically considered central regulators of physiologic lipid storage
194 and turnover, lipid metabolism and signaling are well-known to be essential for the maintenance
195 of optimal β cell insulin release[30,31]. Importantly, mitochondrial lipid metabolism has not been
196 examined in SC-islets to date. We observed distinct subsets of genes related to fatty acid
197 biosynthesis and β-oxidation that were enriched in human islets but were not increased during
198 differentiation towards stage 6 SC-islets (Fig. 5A-B). Specifically, we found genes encoding key
199 initial steps in fatty acid biosynthesis and β-oxidation were markedly lower in SC-islets compared
200 to human islets, including *ACACB*[32,33], a key component of acetyl CoA carboxylase, which
201 catalyzes conversion of acetyl CoA to malonyl CoA as an early step in fatty acid biosynthesis,
202 *CPT1A*[32,34], the rate-limiting enzyme of fatty acid oxidation that catalyzes the transfer of the long-

203 chain acyl-CoA ester to carnitine, to allow fatty acids to enter the mitochondrial matrix for
204 oxidation, and *ACAT1*[34,35], which catalyzes the final step of mitochondrial β-oxidation (Fig. 5C).
205 To assess if differentiating SCs and SC-islets possessed alterations in mitochondrial fatty
206 acid metabolism, we examined acylcarnitine species by LC-MS, as carnitine is a required cofactor
207 for lipid transport into the mitochondria for fatty acid β-oxidation[36]. Notably, we could not detect
208 long-chain acylcarnitines or L-carnitine during differentiation, while these were detectable in
209 human islets (Fig. 5D-E). We next noted low levels of short-chain acylcarnitines throughout SC
210 differentiation, with elevations in short-chain acylcarnitines by stage 6. However, both short- and
211 long-chain acylcarnitines were significantly reduced throughout differentiation to SC-islets when
212 compared to human islets (Fig. 5E). Furthermore, we observed lower expression of *ALDH9A1*, a
213 gene encoding a carnitine biosynthetic enzyme, as well as in *CPT1A*, the key regulator of long-
214 chain acylcarnitine synthesis, in SC-islets compared to human islets, yet other regulators of short-
215 chain acylcarnitine synthesis and other genes in the carnitine biosynthetic pathway were not lower
216 in SC-islets (Fig. 5C and 5F). Of note, L-carnitine is not included within either SC-islet[4] or human
217 islet media formulations, thus these differences were unrelated to L-carnitine supplementation (B.
218 Haight, Prodo Laboratories, personal communication as human islet media formulation is
219 proprietary). These data indicate that in addition to limitations in expression of the ETC-OXPHOS
220 system, SC-islets exhibit robust differences in mitochondrial fatty acid metabolism compared to
221 primary human islets.
222 To ensure our transcriptomic findings were not limited to differentiation of a single hES
223 line, we performed RNA-seq in stage 0-6 cells generated from the HUES8 hES cell line and
224 compared these results to primary human islets. We again observed the expected expression of
225 stage-specific differentiation markers and limitations of islet hormones and of β and α cell
226 maturation markers in stage 6 cells, similar to our observations in H1 cells (Fig. S2A-C). Further,
227 we observed lower expression of key regulators related to fatty acid β-oxidation, glucose transport
228 and glycolysis genes, and genes encoding subunits of all 5 ETC complexes, complex assembly

229 factors in stage 6 SC-islets compared to primary human islets (Fig. S2D-F). In sum, these data
230 indicate that SC-islets have several limitations in mitochondrial programming, including within the
231 ETC-OXPHOS system and mitochondrial fatty acid metabolism.
232
233 **SC-islets display lower expression of PPARα and PPARγ transcriptional targets**
234 Due to the transcriptional differences in the OXPHOS machinery and mitochondrial lipid
235 metabolism, we hypothesized that limitations in key transcriptional pathways might prevent
236 optimal mitochondrial programming in SC-islets. To identify candidate transcriptional regulators,
237 we employed the bioinformatic algorithm Enrichr[37–39] to analyze differentially expressed Mitocarta
238 3.0 genes between stage 6 SC-islets and human islets (Fig. 6A-B). This analysis yielded several
239 expected findings, including the estrogen-related receptor (ERR) family, PDX1, and PRDM16,
240 which all have been associated with the regulation of β-cell development, as well as several
241 effects on mitochondria, including mitochondrial biogenesis, mitophagy, or induction of oxidative
242 metabolism[11,40–43]. We were also intrigued by the enrichment of PPARα and PPARγ in SC-islets,
243 nuclear receptors that are both tightly connected with mitochondrial function, including the
244 regulation of fatty acid oxidation, mitochondrial biogenesis, and coordination of mitochondrial
245 programming together with the co-activator PGC1α, a central regulator of mitochondrial
246 metabolism[44–46]. Thus, we next assessed the expression of PPARα and PPARγ target genes in
247 stage 6 SC-islets and human islets as PPARα and PPARγ had not been previously studied during
248 SC-β cell differentiation. We found that expression of canonical PPARα and PPARγ target genes
249 were lower in stage 6 SC-islets compared to human islets (Fig. 6C). Further, PPARα regulates
250 carnitine biosynthesis and transcriptionally regulates expression of *ALDH9A1*[47,48], which is also
251 lower in SC-islets compared to human islets, as noted above (Fig. 5F).
252 We next wished to determine the mechanisms by which PPAR transcriptional pathways
253 are lower in SC-islets. PPARα classically complexes with RXR, and together with PPAR and RXR

254 ligands and transcriptional co-activators, form a transcriptional complex that can bind PPAR
255 response elements to facilitate target gene expression[49]. Thus, we first assessed expression of
256 the PPAR and RXR transcriptional machinery in stage 6 SC-islets. We found that *PPARA*,
257 *PPARG*, *RXRA*, and *RXRB* expression levels were higher in stage 6 SC-islets compared to
258 human islets (Fig. 6D). While we found that PPARα protein levels appeared to rise throughout
259 differentiation, PPARα protein levels appeared unchanged in stage 6 SC-islets compared to
260 human islets (Fig. 6E). The expression of the PPAR-related co-activators *NCOA1*, *EP300*, *EIF4E*,
261 *SRC*, and *CTNND1* were also more highly expressed in stage 6 SC-islets compared to the human
262 islets (Fig. 6D). To determine if these findings also occurred specifically in β cells, we reanalyzed
263 a publicly-available single-cell RNA-seq data set[28] and found that expression of the *PPARA* and
264 *RXRA* were significantly higher in SC-β cells compared to primary human β cells (Fig. 6F).
265 Further, while we observed lower expression of (*PPARG1A*/*PGC1α*) in SC-islets, we did not
266 observe differences in *PGC1α* expression between SC-β cells and primary human β cells (Fig.
267 6D and F). To assess if chromatin accessibility at putative PPAR- and RXR-binding sites was
268 affected in SC-β cells, we next reanalyzed publicly-available single-cell ATAC-seq data from SC-
269 β cells and primary human β cells[28]. We found that PPAR and RXR motifs were highly accessible
270 in SC-β cells compared to primary β cells (Fig. 6G). These results suggest that limitations in the
271 PPARα/γ transcriptional program in SC-β cells was not due to a loss of the PPAR transcriptional
272 machinery or chromatin accessibility.

273 We next identified a differentiation trajectory of stage 6 SC-β cells using publicly-available
274 single-cell RNA-seq and single-cell ATAC-seq data[28] to understand the dynamics of PPARα
275 expression and activity during β cell differentiation. Using single-cell RNA-seq expression data
276 specifically from stage 6 SC-islet cells, we first identified a developmental trajectory from
277 immature *INS*$^+$ β cells co-expressing the key endocrine progenitor transcription factor *FEV* to more
278 mature β cells with higher *INS* expression and low/absent expression of *FEV* (Fig. S3A-B). Stage
279 6 SC-β cell trajectory was then extracted and combined with single-cell RNA-seq data from

280 primary human β cells to compare expression. We then evaluated several β cell transcriptional
281 regulators, observing greater expression in *PDX1* and *PAX6* across the SC-β cell differentiation
282 trajectory (Fig. S4A). Similarly, *PPAR*α expression increased along the SC-β cell differentiation
283 trajectory (Fig. 6H). Despite this, we observed that the PPARα gene signature score, calculated
284 using the expression of 51 known PPARα transcriptional targets[50], remained at a lower level than
285 primary human β cells throughout the SC-β cell differentiation trajectory (Fig. 6I). We next used
286 ChromVAR[51], a computational approach to estimate a per-cell bias-corrected measure of the
287 change in chromatin accessibility in sets of peaks containing the same transcription factor motif
288 compared to an average cell profile, which serves as a proxy for motif activity. Again, an evaluation
289 of known β cell transcriptional activators revealed increases in *NEUROD1* and *PAX6* motif
290 deviation across SC-β cell differentiation trajectory (Fig. S4B). Intriguingly, we observed that the
291 estimated PPARα motif deviation did not change significantly across the SC-β cell differentiation
292 trajectory but was consistently greater than that of primary β cells (Fig. 6J). Taken together, our
293 analysis of bulk RNA-seq, pseudo-bulk single-cell RNA-seq and single-cell ATAC-seq, and
294 transcriptomic and chromatin accessibility profiling across the SC-β cell differentitation trajectory,
295 all revealed that SC-β cells possess lower expression of target genes within the PPARα pathway
296 that do not appear to be due to reduced expression of the PPAR transcriptional machinery,
297 accessibility of PPAR-binding motifs, or PPARα motif activity.
298
299 **WY14643 improves the differentiation of SC-β cells**
300 While the actions of PPARα/γ are well known in many cell types, including studies in postnatal β
301 cells[52,53], the importance of PPARα/γ during β cell differentiation are unclear. We speculated that
302 the limited activation of PPARα/γ-related mitochondrial programming could be related to the lack
303 of PPARα/γ ligands during SC-islet differentiation. Notably, the primary ligand for RXR is retinoic
304 acid, which is routinely included in SC-islet differentiation protocols[4,54]. Ligand binding to PPARs

305 induces a conformational change that displaces co-repressors and enhances binding to co-
306 activators to promote the expression of target genes[55,56]. PPAR agonists have also been shown
307 to not be required to increase the number of PPARγ-binding sites, suggesting that chromatin
308 accessibility at PPAR motifs in SC-β cells could be maintained and poised for activation in the
309 absence of an agonist[57], consistent with our observations above (Fig. 6F and I). Therefore, we
310 hypothesized that addition of a PPAR agonist may improve SC-β cell differentiation.

311 As a proof of concept, we chose to include the potent PPARα agonist WY14643[58–61] during
312 stage 6 of the differentiation program given our observations of a relative lack of PPARα target
313 gene expression throughout the SC-β cell maturation trajectory despite a maintenance of PPARα
314 motif activity (Fig. 6I-J and 7A). Intriguingly, we found that WY14643 treatment significantly
315 increased the percentage of C-peptide-positive SC-islets without changes to the glucagon-,
316 somatostatin-, or polyhormone-positive cell populations (Figs. 7B). WY14643 treatment also
317 significantly raised the frequency of NKX6.1 and C-peptide co-positive SC-β cells with similar
318 increases in PDX1 and C-peptide co-positivity (Fig. 7C-D).

319 To gain further insight into the mechanisms underlying the expansion of SC-β cells upon
320 PPAR agonism, we performed bulk RNA-seq studies on WY14643-treated SC-islets compared to
321 control-treated SC-islets. Firstly, we observed the expected induction of a subset of PPARα
322 targets in WY14643-treated SC-islets compared to control-treated SC-islets (Fig. 7E). We next
323 observed higher expression of genes reported to be expressed in mature β cells[62] upon WY14643
324 exposure, including *INS*, *UCN3*, *GCK*, and *G6PC2*, as well as lower expression of genes enriched
325 in immature β cells[62], which could also be reflective of a higher percentage of β cells overall in
326 bulk assessments of WY14643-treated SC-islets (Fig. 7F-G). In addition, we found greater
327 expression of ETC-OXPHOS-related genes, with minimal changes in expression of genes related
328 to glucose uptake and glycolysis, in WY14643-treated SC-islets compared to control-treated SC-
329 islets (Fig. 7H-I). Further, we found that addition of WY14643 significantly improved insulin
330 secretion in SC-islets compared to controls, yet the fold induction of insulin secretion by glucose

331 was similar between the groups (Fig. 7J). Together, these studies suggested that WY14643
332 improves the formation of SC-β cells.

333 We next evaluated potential mitochondrial mechanisms promoting SC-β cell formation
334 following WY14643 exposure. We first found modest increases in mitochondrial respiration
335 following high glucose stimulation in WY14643-treated SC-islets (Fig. 7K). We observed that
336 WY14643 treatment resulted in greater protein expression of the complex I subunit NDUFA9
337 compared to controls, however, changes in other OXPHOS subunits were not found (Fig. 7L and
338 S5A). We also observed no changes in mitochondrial mass, expression of regulators of
339 mitochondrial dynamics, or mitochondrial ultrastructure following WY14643 exposure (Figs. 7L
340 and S5B-D). We next found that that WY14643 exposure reduced both fatty acid and acylcartinine
341 concentrations in SC-islets, consistent with the induction of fatty acid oxidation following PPARα
342 agonism (Fig. S6A-B). To evaluate the contributions of mitochondrial pyruvate transport or long
343 chain fatty acid oxidation to the effects of WY14643 on SC-β cell formation, we exposed stage 6
344 SC-islets to WY14643 (or vehicle control) for 7 days in the presence or absence of the
345 mitochondrial pyruvate carrier (MPC) inhibitor UK5099 or the CPT1A inhibitor etomoxir. Indeed,
346 UK5099 exposure abrogated the effects of WY14643 to increase the frequency of SC-β cells,
347 while etomoxir exposure increased the presence of GCG+ SC-α cells (Fig S6E-F). Finally, we
348 examined other metabolic signaling pathways, including Calcium/calmodulin-dependent protein
349 kinase II (CaMKII), AMP-activated protein kinase (AMPK), and acetyl co-A carboxylase (ACC),
350 yet did not observe differences in the phosphorylation and activation of these pathways following
351 WY14643 exposure (Figure S6G-I). Taken together, these results suggest that WY14643 induces
352 both mitochondrial oxidative and fatty acid metabolism to promote SC-β cell formation.

353 We next wanted to determine if the beneficial effects of WY14643 were visible in other SC
354 lines and also durable *in vivo* following transplantation. We first tested the effects of WY14643 in
355 stage 6 SC-islets differentiated from the 19-9-11 induced pluripotent stem cell (iPSC) line (Figure
356 S7A-B). We observed that addition of WY14643 for 7 days increased the insulin secretion index

357 of iPSC-derived SC-islets (Fig. S7C). Next, we treated SC-islets (from the H1 ESC line) with
358 WY14643 or vehicle control for 7 days *in vitro* prior to seeding SC-islets on a poly(lactide-*co*-
359 glycolide) (PLG) microporous scaffold prior to transplantation into the epididymal fat pad of
360 immunodeficient NOD-*scid* IL2Rg^{null} (NSG) mice. We delivered SC-islet grafts to the epididymal
361 fat pad rather than the renal subcapsular space as the epididymal fat pad is a translationally
362 relevant transplant site[63,64] (Fig. 8A). We then retrieved the scaffolds 10 days posttransplant due
363 to the limited half-life of WY14643, and we did not administer WY14643 *in vivo* to avoid systemic
364 effects of the agonist. Following graft retrieval, we observed SC-islets appeared as expected
365 within the scaffold with recipient cell growth within and surrounding the xenograft (Fig. 8B).
366 Notably, we observed a durable effect of WY14643 on the SC-β cell lineage 10 days post-
367 transplantation, with a significant increase in C-peptide-positive SC-β cells compared with vehicle-
368 treated controls (Fig. 8C-D). Further, we observed that WY14643 did not affect the percentage of
369 somatostatin- or glucagon-positive cells but did lead to a modest reduction in the immature
370 polyhormone-positive cell population post-transplantation (Fig. 8C-D). Moreover, WY14643
371 treatment led to a significant increase in insulin content within the explanted scaffold graft
372 compared to vehicle-treated controls (Fig. 8E). We also observed that WY14643 treatment did
373 not significantly alter the frequency of Ki-67/C-peptide co-positive cells, suggesting WY14643
374 likely did not enhance SC-β cell replication (Fig. 8F). WY14643 treatment also did not alter
375 mitochondrial morphology in SC-β cells post-transplantation (Fig. 8G). Taken together, the
376 addition of a PPARα agonist to stage 6 SC-islets improved the formation of SC-β cells, which was
377 durable *in vivo* post-transplantation.
378

379 **DISCUSSION**

380 Here, we reveal a vital importance for mitochondrial programming to promote the differentiation
381 of SC-β cells. Our studies elucidate specific mechanisms underlying limitations in SC-β cell
382 mitochondrial metabolism, including reductions in expression and function of the ETC-OXPHOS

383 system and mitochondrial fatty acid metabolism. We observe limitations in glucose-stimulated
384 respiration in SC-islets without alterations in mitochondrial mass, structure, mtDNA content, and
385 mtDNA replication. We identify several candidates that may contribute to limitations in
386 mitochondrial programming during SC-β cell maturation, notably the nuclear receptors PPARα
387 and PPARγ. We demonstrate that the PPARα and PPARγ transcriptional machinery is intact and
388 chromatin at the sites of PPARα and PPARγ binding motifs is accessible, but expression of PPARα
389 and PPARγ target genes is reduced, suggesting a deficiency of PPAR ligands in the SC-islet
390 differentiation process. To test a proof of concept of the importance of PPAR-mediated
391 programming in SC-β cells, we found that the PPARα agonist WY14643 improved mitochondrial
392 respiration, fatty acid oxidation, and importantly, insulin secretion. Moreover, WY14643 increased
393 the formation of C-peptide-positive SC-β cells both *in vitro* and upon transplantation within a
394 translationally relevant engraftment site, as well as enhancing insulin content within SC-islet
395 grafts. Thus, our data reveal the potential for targeting PPARα-dependent mitochondrial
396 programming to improve SC-β cell differentiation, expanding beyond classical roles for
397 mitochondria simply as a client organelle necessary for β cell bioenergetics.

398 Our results suggest that the activation of mitochondrial transcriptional programs can
399 expand the SC-β cell lineage. While the synchronistic connections between mitochondria and cell
400 fate are well appreciated in other tissue types, such as brown adipocytes[65,66], this connection has
401 not been clear during β cell differentiation. Interestingly, PPARα/γ regulate the differentiation of
402 adipocytes, keratinocytes, bone, and several immune cell types and promote the expression of
403 genes related to lipid metabolism and mitochondrial biogenesis[67–73], yet their function in SC-β cell
404 differentiation had not previously been observed. In adult human islets, PPARα overexpression
405 or treatment with a PPARα agonist offered protection from lipotoxicity and preserved GSIS[74,75].
406 Similarly, PPARγ agonists preserved β cell function in humans with T2D and protected human
407 islets from lipotoxicity[52,76–78]. However, a role for mitochondrial programming by PPARα/γ to

408 promote human β cell differentiation was not examined. Our studies reveal the potential for
409 targeting PPARα to improve mitochondrial respiration and fatty acid metabolism and expand the
410 SC-β cell lineage. Indeed, we speculate that PPARα could act through mitochondria to promote
411 β cell differentiation by supporting the bioenergetic demands of differentiation or through
412 increased substrate availability to facilitate histone modifications and chromatin accessibility at
413 key β cell differentiation genes, which remains to be tested in the future. Future work will also be
414 needed explore the addition of PPAR agonists in other SC-β cell differentiation stages, define the
415 roles of PPARs on metabolism throughout β cell development, and to explore the potential for
416 shared PPAR-related mechanisms underlying differentiation across tissues, including SC-β cells
417 as well as adipocytes, keratinocytes, bone, and immune cells.

418 PPARα/γ are well known regulators of lipid metabolism, and PPARα is a central regulator
419 of fatty acid oxidation. Our studies suggest that WY14643 enhances both mitochondrial fatty acid
420 oxidation and respiration in SC-islets. Beyond their roles in lipid metabolism and mitochondrial
421 biogenesis, emerging studies demonstrate crosstalk between ERRα and PPARα, which could
422 suggest the potential that WY14643 might indirectly support expression of OXPHOS targets
423 through ERRs[44,79]. Our studies define a previously unknown impairment in mitochondrial lipid
424 metabolism in SC-islets with beneficial roles of WY14643 on SC-β cell formation, as well as
425 OXPHOS gene expression, which appears distinct from the roles of ERRγ to improve SC-β cell
426 GSIS through induction of OXPHOS and suppression of glycolysis[11]. Future studies will be crucial
427 to discriminate both the specific and integrated contribution of each of these highly integrated
428 mitochondrial transcriptional regulators on SC-islet development, including PPARα, PPARγ,
429 ERRγ, and PGC1α. The impact of pharmacologic agonists of ERRγ[80] and specific, partial, or dual
430 agonists of PPARα and PPARγ[81–83], to together improve both SC-β cell differentiation (through
431 PPARα) and maturation/GSIS (through ERRγ) will be intriguing to assess for future translational
432 benefit.

433 Our studies expand upon the metabolic differences observed in SC-islets compared to
434 primary human islets, which have understandably focused to date on glucose metabolism given
435 the pivotal importance of glucose metabolism for β cell insulin secretion. We found that SC-islets
436 do not increase mitochondrial respiration upon high glucose stimulation, similar to the
437 observations of others[6,10]. We noted that SC-islets exhibited both lower oxygen consumption
438 following oligomycin exposure and a higher peak oxygen consumption after the uncoupler FCCP
439 compared to human islets, which had not been observed previously. These effects could be a
440 function of differences of tissue penetration of pharmacologic agents between SC-islets and
441 human islets despite their similar size and appearance. Alternatively, the differences in SC-islet
442 responses to oligomycin and FCCP could be indicative that SC-islets may be more coupled or
443 possibly have reductions in proton leak compared to primary human islets. Primary β cells are
444 known to be remarkably uncoupled, and blockade of adenosine nucleotide translocase (ANT)-
445 mediated basal proton leak impairs GSIS[84–87]. Indeed, SC-islets express significantly lower levels
446 of ANT than primary human islets ($\log_2$FC -0.66, FDR < 0.05). We also observe alterations in
447 mitochondrial acylcarnitine profiles in SC-islets, indicative of limitations in mitochondrial lipid
448 metabolism that may originate due to limitations in mitochondrial programming by PPARα/γ. A
449 recent study demonstrated that elevations in the sphingolipid ceramide limited the maturation of
450 SC-β cells, suggesting that other lipid subtypes may play distinct roles in differentiation[88].
451 Reduced levels of C3 and C5 acylcarnitines may also reflect alterations in branched chain amino
452 acid metabolism[89], an effect we also observed in SC-islets (Fig. 3D). Notably, fluctuations in amino
453 acid availability at birth may also impact the nutrient sensitivity of mTORC1 signaling pathway to
454 affect β cell maturation[90]. Unsaturated fatty acids can serve as endogenous ligands for PPARα
455 and/or PPARγ, leading us to speculate a possible similar role for these metabolites in β cell
456 maturation, especially given the fatty acid composition of maternal breast milk[91–94]. It will be
457 intriguing to test if future approaches to modulate β cell uncoupling or nutrient exposure will have
458 a beneficial impact on SC-β cell differentiation and maturation. On the other hand, exploration of

459 the SC-islet microenvironment or culture conditions, could provide an alternative approach to
460 clarify the metabolic control of SC-β cell differentiation and function.

461 Limitations in our study included use of RNA-seq data performed on bulk SC-islet
462 differentiations, which have a different cell type composition than bulk primary human islets[28]. Our
463 conclusions were supported, however, by re-analysis and inclusion of published single cell RNA-
464 seq of SC-β cells and primary β cells[28]. Further, despite reports of mitochondrial dysfunction in
465 SC-islets from numerous groups, the effect of PPAR agonists will need to be evaluated in other
466 SC-β cell differentiation protocols, as our observations could be protocol-dependent. While
467 numerous studies, including genetic knockout models, indicate a specific role for WY14643 both
468 *in vitro* and *in vivo* through PPARα[59–61], WY14643 has been reported to have weak PPARγ activity
469 *in vitro*[95]. Thus, additional studies to dissect the contribution of PPARγ on SC-islet differentiation
470 would be valuable in the future. An additional limitation of our study is the need to determine if
471 PPAR agonism, such as by WY14643 or other agents, is able to promote SC-β cell differentiation
472 and function to ultimately improve glycemic control upon engraftment in diabetic mice *in vivo*. We
473 also did not explore the role for systemic administration of PPAR agonists post-transplantation,
474 which might provide additional opportunities to enhance *in vivo* SC-β cell function.

475 Our findings support metabolic limitations previously found in the generation of SC-β cells,
476 but also open new roles for of PPARα and mitochondria in the regulation of SC-β cell
477 differentiation. Our results reinforce the findings of several studies of SC-β cell metabolism,
478 including defects in OXPHOS expression, persistence of aberrant glycolytic metabolism, and
479 limitations in expression of the ERR transcriptional pathway[6,10,11], while clarifying new roles for
480 mitochondrial fatty acid metabolism and OXPHOS mediated at least in part by PPARα. Our results
481 also demonstrate the novel potential to activate PPARα as a highly druggable target to improve
482 SC-β cell differentiation. Taken together, our results corroborate limitations that remain in the
483 formation of SC-β cells and identify new potential routes to overcome these deficits, possibly
484 requiring pharmacologic targeting of several complementary pathways to generate higher

485 quantities of fully functional SC-β cells for enhanced therapeutic use in diabetes. Early clinical
486 trials have provided excitement regarding the therapeutic potential for SC-islet transplantation to
487 provide a functional cure for T1D[3,96]. However, these allografts require up to 6 months to optimize
488 their function, and the long-term viability of these cells remain unclear[3]. Thus, our studies highlight
489 the opportunity to focus on mitochondrial programming pathways to improve the differentiation,
490 metabolism, and function of SC-β cells to more closely resemble primary β cells as an approach
491 to improve durable cell-based therapies for T1D.
492

493 **EXPERIMENTAL MODEL AND SUBJECT DETAILS**

494 **Stem cell-derived islets (SC-islets):** SC-islets were differentiated from H1, HUES8, and IPS-DF
495 19-9-11 T.H (feeder independent; WiCell) human pluripotent stem cells (hPSCs) using a 6-stage
496 protocol, as reported previously[4,63,64,97]. Briefly, undifferentiated cells were dispersed into single
497 cells, and 5 × 10^6 cells were seeded in 6-well cell culture treated plates coated with Matrigel
498 (Corning). Cells were cultured for 24 h in mTeSR1 and then cultured in the differentiation media
499 for 6 stages. During each stage, cells received daily media changes with stage-specific basal
500 media supplemented with growth factors and small molecules to induce differentiation. The stages
501 of this protocol are defined as definitive endoderm (stage 1), primitive gut tube (stage 2),
502 pancreatic progenitor (stages 3 and 4), endocrine progenitor (stage 5) and immature stem cell
503 derived β-cell (stage 6). At the end of each stage, cells could be dissociated from the plate, fixed
504 and analyzed using intracellular flow cytometry for stage-specific biomarkers. For reaggregation
505 from planar culture, cells were dispersed into single cells using TrypLE and seeded onto
506 suspension culture 6-well plates at 8 × 10^6 cells per well. Y27632 was included in the media for
507 the first 24 hours of culture, then media was changed every other day for the duration of culture.
508 Plates were placed on an orbital shaker set to 100 rpm inside a humidified incubator. Reaggregted
509 cell clusters were treated with 60 μM WY14643 alone or with 4 μM UK5099 or 25 μM Etomoxir
510 days 3-10. For scaffolds, reaggregated cell clusters were collected and seeded on the scaffold
511 in the same manner as described above after 3–4 days in culture,.

512 **Microporous scaffold fabrication**: Poly(lactide-*co*-glycolide) (PLG) microporous scaffolds were
513 fabricated as previously described[63]. Briefly, PLG microporous scaffolds were fabricated by
514 compression molding PLG microspheres (75 : 25 mole ratio d,l-lactide to glycolide) and 250 to
515 425 μm salt crystals in a 1:30 ratio of PLG microspheres to salt. The mixture was humidified in an
516 incubator for 7 minutes. Scaffolds were compression molded with 77.5 mg of polymer–salt mixture
517 into cylinders 5 mm in diameter by 2 mm in height using a 5 mm KBr die (International Crystal
518 Laboratories, Garfield, NJ) at 1500 psi for 30 seconds. Molded constructs were gas foamed in

519 800 psi carbon dioxide for 16 hours in a pressure vessel. The vessel was depressurized at a
520 controlled rate for 30 min. On the day of cell seeding, scaffolds were leached in water for 1.5
521 hours, changing the water once after 1 hour. Scaffolds were disinfected by submersion in 70%
522 ethanol for 30 seconds and rinsed multiple times with phosphate-buffered saline (PBS).

523 **Scaffold seeding of SC-islets**: To initiate scaffold culture differentiations from reaggregated
524 clusters, reaggregated clusters were seeded on scaffolds at a density of 125×10^6 cells/cm^3. Prior
525 to seeding, scaffolds were washed in cell media solution then briefly dried on sterile gauze to
526 improve the absorption of the cell solution into the scaffold. Cells were distributed across both
527 faces of the scaffold and then incubated for 2 hours to allow cell solution to be further absorbed
528 into the scaffold before differentiation media was added.

529 **Human islets:** All human samples were procured from de-identified donors without diabetes from
530 the Integrated Islet Distribution Program, Alberta IsletCore, or Prodo Laboratories and approved
531 by the University of Michigan Institutional Review Board. Human primary islets were cultured at
532 37°C with 5% CO_2 in PIM(S) media (Prodo Laboratories, Aliso Viejo, CA, USA) supplemented
533 with 10% FBS, 100 U/mL penicillin/streptomycin, 100 U/mL antibiotic/antimycotic, and 1 mM
534 PIM(G) (Prodo Laboratories, Aliso Viejo, CA, USA). Islets were used from male and female
535 donors, and donor information is provided in Table S1.

536 **Transplantation of reaggregated SC-islets in immunodeficient mice**: SC-islets were
537 transplanted as previously described[63]. All mice were maintained in accordance with the
538 University of Michigan's Institutional Animal Care and Use Committee under specific pathogen-
539 free conditions and were assigned randomly to different experimental groups. Up to 5 mice were
540 housed per cage and were maintained on regular chow with *ad libitum* access to food and water
541 on a 12 h light-dark cycle. 8–10-week-old male NOD.Cg-Prkdc^{scid} Il2rgtm1Wjl/SzJ (NSG) mice
542 (Jackson Laboratories) were used for transplantation studies. On the day of transplantation, the
543 abdomen was shaved and sterilized. A small incision was made in the peritoneal wall and the
544 epididymal fat pads were unwrapped outside the body. As described above, reaggregated cell

545 clusters were collected and seeded on both faces of the scaffold and incubated at least 2 h before
546 transplantation. Reaggregated cell-laden scaffolds were placed on the fat pads, wrapped in fat
547 pad tissue, and placed back into the peritoneal cavity. Each mouse received approximately 5
548 million cells in clusters on each scaffold, equaling a total of 10 million cells transplanted per
549 mouse. Mice were sutured, surgically stapled, and received carprofen (0.5 mg/mL) the day of and
550 after surgery. Body weight was measured daily for 10 days prior to euthanasia and subsequent
551 graft harvest.

552 **METHOD DETAILS**

553 **Culture methods:** Human pluripotent stem cell differentiation in H1 and HUES8 cells was
554 performed as per the protocol previously published by Hogrebe, et al. 19-9-11 T.H (feeder
555 independent) induced pluripotent cells were differentiated through stage 4 using the STEMdiff™
556 Pancreatic Progenitor Kit (#05120) and subsequently as above.

557 **Flow cytometry:** Single cell dissociations were fixed in 4% paraformaldehyde and blocked with
558 5% normal donkey serum in 0.1% Triton-X PBS. Cells were incubated overnight with primary
559 antibodies, washed and subsequently incubated with appropriate secondary antibodies. Stained,
560 fixed cells were analyzed by ZE5 cell analyzer (Bio-Rad). Primary and secondary antibodies used:
561 anti-OCT-3/4 (Santa Cruz Biotechnology, catalog # sc-5279), anti-chromogranin A (Invitrogen,
562 catalog # PIMA533052), anti-C-peptide (Developmental Studies Hybridoma Bank, University of
563 Iowa, catalog # GN-ID4-S), anti-NKX6–1 (Developmental Studies Hybridoma Bank, University of
564 Iowa, catalog # F55A12-S), anti-PDX1 (R&D Systems, catalog #AF2419), AlexaFluor 488
565 (Invitrogen, catalog # A21208), AlexaFluor 488 (Invitrogen, catalog # A21202), AlexaFluor 647
566 (Invitrogen, catalog # A31571), AlexaFluor 647 (Invitrogen, catalog # A21447), AlexaFluor 647
567 (Invitrogen, catalog # A31573).

568 **Static *in vitro* insulin secretion measurements:** Static insulin secretion assays on human islets
569 and SC-islets were performed following 1 h incubations with 1.67 mM and 16.7 mM glucose, and
570 30mM KCl in HEPES-supplemented KRB buffer containing 135 mM NaCl, 4.7 mM KCl, 1.2 mM

571 KH_2PO_4, 5 mM $NaHCO_3$, 1.2 mM $MgSO_4.7H_2O$, 1 mM $CaCl_2$, 10 mM HEPES and 0.1% BSA (pH
572 7.4). Samples were analyzed for insulin release using Human Insulin Chemiluminescence ELISA
573 (ALPCO; Salem, NH, USA) as per the manufacturer's protocol.
574 **Insulin content of explanted scaffolds:** Explanted scaffolds were placed in 9.1 mM HCl 95%
575 EtOH solution. For extraction, samples were sonicated 5x for 15 sec, resting on ice in between
576 sonication periods. Samples were rotated at 4°C overnight. Samples were then spun at 2500
577 RPM for 30 min at 4°C. Supernatants were stored at -80°C until analysis. Samples were analyzed
578 for insulin release using Human Insulin Chemiluminescence ELISA (ALPCO; Salem, NH, USA)
579 as per the manufacturer's protocol.
580 **Mitochondrial respirometry:** The oxygen consumption rate was measured in stage 6 SC-islets
581 and primary human islets using the BaroFuse (EnTox Sciences, INC; Mercer Island, WA, USA)
582 as previously described[20]. 200 islets were placed in Krebs-Ringer Bicarbonate HEPES (KRBH)
583 buffer with a 2 mM glucose per condition. Islets were subject to the following conditions: 20 mM
584 glucose, 10 μM oligomycin (Sigma), 1 μM FCCP (Sigma-Aldrich), and 3 mM KCN (Thermo
585 Scientific) for 60 min each.
586 **Metabolomics:** Cells were cultured according to Hogrebe et al[4]. On the day of sample collection,
587 samples were incubated in MCDB 131 with 10.5 g BSA, 5.2 mL GlutaMAX, 5.2 mL P/S, 5 mg
588 heparin, 5.2 mL MEM nonessential amino acids (Corning, 20–025-CI), 84 μg ZnSO4
589 (MilliporeSigma, 10883), 523 μL Trace Elements A (Corning, 25–021-CI), and 523 μL Trace
590 Elements B (Corning, 25–022-CI) and either 5.5mM or 20mM glucose for 3 hr. Media was
591 removed, and the cells were washed 1X with ice-cold 150 mM ammonium acetate in LC-MS grade
592 water. Cells were harvested with 200 μL of ice-cold methanol and frozen at -80°C until sample
593 preparation. For extraction, 200 μL of cold water was added to the cells and the cells were
594 scraped. The resulting homogenate was sonicated on ice for 10 sec. 400 μL of chloroform was
595 added. Samples were centrifuged at 17,000 x *g* for 10 min and the resulting top layer was
596 collected and taken to dryness under nitrogen. Samples were reconstituted in 30 μL of 2:1 ACN:

597 water, filtered and 5 µL were injected for analysis. The samples were separated as previously
598 described[98]. LC-MS analysis was performed on the Agilent 6546 quadrupole TOF mass
599 spectrometer, which was coupled to Agilent 1290 LC. The gas temperature was set at 225°C, the
600 drying gas flow at 10 L/min, the nebulizer at 40 psi, the sheath gas temperature at 300°C, and the
601 sheath gas flow at 12 L/min. The Fragmentor (Agilent) was set at 125 V, the skimmer at 65 V, and
602 VCap at 3,000 V. For verification of metabolite identity and retention time, authentic standards of
603 all measured metabolites were run separately and spiked into pooled samples. Metabolites were
604 separated on an InfinityLab Poroshell120 HILIC-Z, 2.7 µm, 2.1 × 150 mm column (Agilent
605 Technologies, CA, USA). Mobile phase A was composed of 90% 10 mM ammonium acetate pH
606 9.0 with ammonia, 10% acetonitrile (ACN) with 2.5 uM InfinityLab Deactivator Additive (Agilent
607 Technologies, CA, USA) and mobile phase B was composed of 15% 10 mM ammonium acetate
608 pH 9.0 with ammonia, 85% acetonitrile with 2.5 uM InfinityLab Deactivator Additive. The flow rate
609 was 0.25 mL/min, and the gradient was as follows: 0-2 min at 95 % B, 2-5 min at 95% B, 5-5.5
610 min at 86%, 5.5-8.5 min at 86% B, 8.5-9 min at 84% B, 9-14 min at 84% B, 14-17 min at 80% B,
611 17-23 min at 60% B, 23-26 min at 60% B, 26-27 min at 95% B, and 27-35 min at 95% B. Column
612 compartment temperature was kept at 25 °C. Data were acquired in negative mode.
613 **Lipidomics:** Media were removed, and metabolites were extracted with solvent (8:1:1 ratio of
614 methanol/Chloroform/water) containing stable isotope-labeled internal standards. As previously
615 described[99], an Agilent 6410 triple quadrupole MS system equipped with an Agilent 1200 LC
616 System and an ESI source was utilized. Metabolite separation was achieved using gradient
617 elution on a reverse phase XBridge C18 Column (50 mm × 2.1 mm, 2.5 µm, Waters, Milford, MA,
618 USA) with the corresponding guard column (5 mm x 2.1 mm, 1.7 µm) maintained at 40 °C. LC
619 vials were maintained at 4 °C in a thermostatic autosampler, and the injection volume was set at
620 4 µL. The mobile phase consisted of solvent A, 5 mM Ammonium Acetate, and solvent B,
621 Acetonitrile. The flow rate was 0.25 mL/min. The gradient elution program was as follows: 0–8.50
622 min, 2% B; 1.5–9 min, linear gradient from 2% to 50% B; 9–14 min, linear gradient from 50% to

623 95% B; hold at 95% B for 3 min. The flow rate was 300 µL/min. Acylcarnitine species were each
624 detected by their characteristic LC retention time in the MRM mode following ESI and comparing
625 relative areas with those of corresponding standards. Concentrations of carnitine, acetylcarnitine
626 (C2), propionylcarnitine (C3), butyrylcarnitine (C4), isovalerylcarnitine (C5), hexanoylcarnitine
627 (C6), octanoylcarnitine (C8), myristoylcarnitine (C14), palmitoylcarnitine (C16), and
628 oleoylcarnitine (C18) were calculated by ratios of peak areas of known concentrations of stable
629 isotopically-labeled analogs.

630 **mtDNA content and replication assessments:** 25 human islets per donor were handpicked and
631 washed twice with 1X PBS. 100,000 cells from differentiation stage 0 through 6 were washed
632 twice with 1X PBS. Human islets and stem cells were pelleted and stored at -80°C until DNA
633 extraction using the Blood/Tissue DNeasy kit (Qiagen; Germantown, MD, USA) as per
634 manufacturer's instructions. Relative mtDNA content was quantified by qPCR using mtDNA
635 specific primers ND1 (5'-ACCCCCTTCGACCTTGCCGA-3' and 5'-
636 GGGCCTGCGGCGTATTCGAT-3'), and nuclear DNA specific primers for GAPDH (5'-
637 AATCCCATCACCATCTTCCA-3' and 5'-TGGACTCCACGACGTACTCA-3') as previously
638 described[100]. First-strand mtDNA replication levels were measured by qPCR following digestion
639 by Mnl I, which site specifically digest double-stranded DNA[101,102]. Briefly, primers specific to 7 S
640 mtDNA (5′-ATCAACTGCAACTCCAAAGCCACC-3′ and 5′-TGATTTCACGGAGGATGGTGGTCA-
641 3′), whose amplicon contains a Mnl I site, were used to quantify relative single-stranded mtDNA
642 forming the D-loop. Single-stranded DNA generated from the extension of 7S region was
643 measured using primers specific to CYTB (5′-AGTCCCACCCTCACACGATTCTTT-3′ and 5′-
644 AGTAAGCCGAGGGCCTCTTTGATT-3′), which also contains an Mnl I site. Primers specific to
645 COXI (5′-ACCCTAGACCAAACCTACGCCAAA-3′ and 5′-TAGGCCGAGAAAGTGTTGTGGGAA-
646 3′), whose amplicon does not contain an Mnl I site, were used to quantify non-replicating double-
647 stranded mtDNA. The ratio of 7S or CYTB amplicons to the COXI amplicon were then calculated

648 after qPCR of Mnl I-digested DNA to determine the relative amount of single-stranded mtDNA at
649 the D-loop strand or initiation of first strand replication, respectively.
650 **Citrate synthase activity assay**: 1,000 human islets per donor were handpicked and washed
651 twice with 1X PBS. One million cells from differentiation stage 0 through 6 were washed twice
652 with 1X PBS. Human islets and stem cells were lysed with radioimmunoprecipitation assay buffer
653 containing protease and phosphatase inhibitors (Calbiochem), and insoluble material was
654 removed by centrifugation. Lysates were used to determine citrate synthase activity with the
655 MitoCheck Citrate Synthase Activity Assay Kit (Cayman Chemical, Catalog# 701040) per
656 manufacturer's instructions.
657 **Western blotting:** 1,000 human islets per donor were handpicked and washed twice with 1X
658 PBS. One million cells from differentiation stage 0 through 6 were washed twice with 1X PBS.
659 Human islets and stem cells were lysed with radioimmunoprecipitation assay buffer containing
660 protease and phosphatase inhibitors (Calbiochem), and insoluble material was removed by
661 centrifugation. Equal amounts of proteins were resolved on 4%–20% gradient Tris-glycine gels
662 (Bio-Rad) and transferred to nitrocellulose membranes (Bio-Rad). Membranes were then blocked
663 in 5% milk for 1 h and immunoblotting was performed using antibodies to Vinculin (1:1000;
664 Millipore, Catalog# CP74), TOM20 (1:1000; Cell Signaling Technology, Catalog# 42406), Total
665 OXPHOS Human Antibody Cocktail (1:1000; Abcam, ab110411), NDUFA9 (1:1000; Abcam;
666 ab14713), UQCRC2 (1:1000; Abcam; ab14745), PPARα (1:3000; ProteinTech; 66826-1),
667 phospho-CAMKII (1:1000; Cell Signaling; 12716), CAMKII (1:50; Santa Cruz; sc-5306), phospho-
668 AMPK (1:1000; Cell Signaling; 2535), AMPK (1:1000; Cell Signaling 2793), phospho-ACC
669 (1:1000; Cell Signaling; 3661), ACC (1:10,000; ProteinTech; 67373-1) and species-specific HRP-
670 conjugated secondary antibodies (Vector Laboratories).
671 **RNA-seq:** Sequencing was performed by the Advanced Genomics Core at University of Michigan
672 Medical School. 250 human islets per donor were handpicked and washed twice with 1X PBS.
673 250,000 cells from differentiation stage 0 through 6 were washed twice with 1X PBS. Total RNA

674 was isolated from human islet and stem cell samples and DNase treated using commercially
675 available kits (Omega Biotek and Ambion, respectively). Libraries were constructed and
676 subsequently subjected to 151 bp paired-end cycles on the NovaSeq-6000 platform (Illumina).
677 FastQC (v0.11.8) was used to ensure the quality of data. Reads were mapped to the reference
678 genome GRCm38 (ENSEMBL), using STAR (v2.6.1b) and assigned count estimates to genes
679 with RSEM (v1.3.1). Alignment options followed ENCODE standards for RNA-seq. FastQC was
680 used in an additional post-alignment step to ensure that only high-quality data were used for
681 expression quantitation and differential expression. Data were pre-filtered to remove genes with
682 0 counts in all samples. Differential gene expression analysis was performed using DESeq2,
683 using a negative binomial generalized linear model (thresholds: log2(fold change) >0.5 or <-0.5,
684 FDR (P_{adj}) <0.05). Plots were generated using variations of DESeq2 plotting functions and other
685 packages with Genialis (Boston, MA, USA).
686 **Pathway analysis of differentially expressed genes:** Differentially expressed genes for each
687 cell-type were identified using DESeq2 packages with Genialis (Boston, MA, USA). The Kyoto
688 Encyclopedia of Genes and Genomes (KEGG), gene ontology (GO), and WikiPathways
689 databases via both Enrichr and STRING databases were used to determine association with
690 particular biological processes, diseases, and molecular functions. The top pathways with an
691 FDR-adjusted *p*-value < 5% were summarized in the results.
692 **Transcription factor analysis of differentially expressed genes:** Differentially expressed
693 genes for each cell-type were identified using DESeq2 packages with Genialis (Boston, MA,
694 USA). ChIP Enrichment Analysis (ChEA) and TF Perturbations Followed by Expression
695 databases via Enrichr were used to determine association with particular biological processes,
696 diseases, and molecular functions. The top pathways with an FDR-adjusted *p*-value < 5% were
697 summarized in the results.
698 **Removal of batch effects between differentiations:** Bias in gene expression values was
699 removed using a tool called ComBat-seq, using protocol selection as batch effect and treatment

700 selection as group effect. ComBat-seq adjusted batch effects in RNA-seq count data. Normalized
701 RNA-seq counts were uploaded into new collections on the Genialis Expressions. The counts
702 were adjusted by mapping the quantiles of the empirical distributions of data to the batch-free
703 distributions[103]. Batch effect adjustment was done using the sva (v3.48.0) R package[104]. The
704 ComBat-Seq method adjusted raw gene counts for differentiation protocol while retaining
705 biological signal from treatment. Batch effect corrected raw counts were TPM normalized using
706 rnanorm (v1.5.1) Python package (https://github.com/genialis/RNAnorm).
707 **Analysis of publicly-available scRNA-seq and scATAC-seq**[28]: Pseudo-bulk analyses were
708 conducted by comparison of log2 (fold change) between SC-β cells compared to primary β cells.
709 For mapping the SC-β cell differentiation trajectory, we downloaded preprocessed multi-omics
710 (paired scRNA-seq and scATAC-seq) data from SC islets and performed quality control on each
711 modality and sample individually and retained only barcodes that passed quality filtering in both
712 modalities. We embedded the cells using 100 highly variable genes based on the transcriptomic
713 modality only with phate[104] and clustered the cells based on the first 2 phate components. Based
714 on marker genes, we identified trajectories from immature to mature endocrine cell types and
715 extracted the β cell lineage and binned cells along the first phate component. For identification of
716 primary human β cells, we downloaded preprocessed multi-omics (paired scRNA-seq and
717 scATAC-seq) data from primary human islets and performed quality control on each modality and
718 sample individually and retained only barcodes that passed quality filtering in both modalities. We
719 embedded the cells using UMAP based on the first 20 Harmony[105] corrected principal components
720 calculated from 2000 highly variable genes based on the transcriptomic modality. We clustered
721 the cells and based on marker genes, retained only primary human β cells, which we
722 concatenated with the cells extracted from the SC-β cell differentiation trajectory. For estimating
723 motif activity, we called peaks based on the ATAC-seq modality with MACS2[106] using the cells
724 extracted from the SC-β cell differentiation trajectory and counted fragments in peaks for both

725 primary and SC-β cells using Signac[107]. We identified motifs using the JASPAR2024 database[108],
726 which we used as input for chromVAR[51].
727 **Transmission electron microscopy:** Human islets and SC-islets were handpicked, fixed in 3%
728 glutaraldehyde and 3% paraformaldehyde in 0.1 M Cacodylate buffer (CB; pH 7.2) at room
729 temperature for 5 min and then stored at 4 °C. Islets were then washed with PBS and centrifuged
730 at 2000 rpm for 2 min. Pre-warmed 2% agarose solution was then carefully added to islet pellets,
731 centrifuged and allowed to cool at 4 °C for 30 min. Samples were then subjected to osmification
732 in 1.5% K4Fe(CN)6 + 2% OsO4 in 0.1 CB for 1 h, dehydrated by serial washes in EtOH (30%,
733 50%, 70%, 80%, 90%, 95% and 100%) and embedded in Spurr's resin by polymerization at 60 °C
734 for 24 h. Polymerized resins were then sectioned at 90 nm thickness using a Leica EM UC7
735 ultramicrotome and imaged at 70 kV using a JEOL 1400 TEM equipped with an AMT CMOS
736 imaging system. Mitochondrial structures (Aspect Ratio, Perimeter, Circularity) were analyzed and
737 quantified by ImageJ.
738 **Immunofluorescence of cryosections**: SC-islets and scaffolds containing SC-islets were
739 picked/excised and fixed in 4% paraformaldehyde for 4 h at 4 °C. SC-islets were washed with
740 PBS and centrifuged at 2000 rpm for 2 min. SC-islets were incubated in methylene blue at room
741 temperature for 20 min and then washed 2x with PBS. Excised scaffolds were washed 3x with
742 PBS for 10 min. SC-islets and scaffolds were stored in 30% sucrose in PBS for 16 h at 4 °C . SC-
743 islets and scaffolds were embedded in OCT and frozen at -80 °C and cryosectioned. SC-islet
744 sections were rinsed with 75% EtOH for 5 min at RT to remove methylene blue. SC-islet and
745 scaffold sections were washed 3x with PBS, permeabilized with 0.2% Triton X-100 in PBS for 15
746 min, washed 3x with PBS and blocked at RT for 1 h with 5% donkey serum in PBT. Primary
747 antibodies were added for 16 h at 4 °C. Primary antibodies raised against C-peptide (1:50; DSHB,
748 Catalog#GN-ID4), Glucagon (1:2000; SantaCruz, Catalog# sc-13091), Glucagon (1:500; Cell
749 Signaling, Catalog#2760), Somatostatin 28 (1:500; Abcam, Catalog#ab111912), Human antigen
750 clone 235-1 (Millipore Sigma; Catalog#MAB1281), OXPHOS (1:100; Abcam, Catalog#ab110411),

751 PDX1 (1:1000; Abcam, Catalog#ab47308), NKX6.1 (1:500; Abcam, Catalog#ab221549), and Ki-
752 67 (1:250, Thermo, Catalog#PA5-19462) were used. Sections were then washed 3x with PBS
753 and incubated for 2 h at room temperature with species-specific Dylight405, Cy2, Cy3, and Cy5-
754 conjugated secondary antibodies (Jackson Immunoresearch). Nuclear labelling was performed
755 using DAPI (Invitrogen). Images were captured under 20X and 60X oil immersion magnification
756 on an Olympus IX81 microscope. Immunostained islets were captured with Z-stack images and
757 subjected to deconvolution (CellSens; Olympus). Hormone-positive cells were quantified as
758 hormone-positive cell/total DAPI-positive (*in vitro*) or Human Ag-positive (post-transplantation)
759 cells. Ki-67-positive cells were quantified as Ki-67-positive/total C-peptide-positive cells.
760 Quantification of hormone-positive and Ki-67-positive cells was carried out with blinded samples,
761 and samples were reidentified after quantification to reduce bias. Quantitative 3-D assessments
762 of mitochondrial morphology and network were performed on ImageJ using Mitochondria
763 Analyzer plugin[102,109].
764 **Statistics:** In all figures, data are presented as mean ± SEM, and error bars denote SEM, unless
765 otherwise noted in the legends. Statistical comparisons were performed using unpaired two-tailed
766 Student's *t*-tests, one-way or two-way ANOVA, followed by Tukey's or Sidak's post-hoc test for
767 multiple comparisons, as appropriate (GraphPad Prism and R). A P value < 0.05 was considered
768 significant. For transcriptomic profiling, a FDR-corrected P value <0.05 were considered
769 significant (see RNA-seq of SC-islets and human islets above). Outlier tests (ROUT method[110])
770 were routinely performed in GraphPad Prism, and all results were included in analysis unless
771 designated by the ROUT method.
772
773 **Data Availability**
774 RNA-seq data have been deposited at GEO (GSE270220). Any additional information required to
775 reanalyze the data reported in this paper is available from the lead author on request.
776

Acknowledgements

S.A.S. acknowledges support from the JDRF (CDA-2016-189, COE-2019-861, SRA-2023-1392), the NIH (R01 DK108921, R01 DK135032, R01 DK135268, R01 DK136671, R01 DK127270, U01 DK127747, P30 DK020572), the Department of Veterans Affairs (I01 BX004444), the Brehm family, and the Anthony family. A.C.L. was supported by the NIH (T32-GM832230). J.L.K. was supported by the National Science Foundation Graduate Research Fellowship (DGE-2241144). G.L.P. was supported by the American Diabetes Association (19-PDF-063). E.L-D. was supported by the NIH (T32-AI007413, T32-AG000114). B.H-K. was supported by the NIH (T32-AI007413, T32-GM145304, F31-DK138544). E.M.W. was supported by the NIH (K01 DK133533). J.G.S.M was supported by the Novo Nordisk Foundation (NNF21OC0068929). S.P. was supported by the JDRF (COE-2019-861) and the NIH (P30DK089503). The JDRF Career Development Award to S.A.S. is partly supported by the Danish Diabetes Academy and the Novo Nordisk Foundation. Next generation sequencing was carried out in the Advanced Genomics Core at the University of Michigan. Human pancreatic islets and/or other resources were provided by the NIDDK-funded Integrated Islet Distribution Program (IIDP) (RRID:SCR _014387) at City of Hope, NIH Grant # U24DK098085. Human islets were also provided by the Alberta Diabetes Institute IsletCore at the University of Alberta in Edmonton (http://www.bcell.org/adi-isletcore.html) with the assistance of the Human Organ Procurement and Exchange (HOPE) program, Trillium Gift of Life Network (TGLN), and other Canadian organ procurement organizations. Islet isolation was approved by the Human Research Ethics Board at the University of Alberta (Pro00013094). All donors' families gave informed consent for the use of pancreatic tissue in research. We thank Drs. K. Claiborn, L. Satin, R. Kennedy, D. Lorberbaum, S. Nowinski, and members of the Soleimanpour laboratory for helpful advice.

Author Contributions

A.C.L. conceived, designed, and performed experiments, interpreted results, drafted, and reviewed the manuscript. E.M.W., J.K., K.C., E.B., A.M.S., J.Z., G.L.P, E.L-D., B.H-K., R.K.D., J.L., Y.W., E.C.R., M.A., V.S., J.P.P., and L.M. designed and performed experiments and interpreted results. T.J.H., M.M.C., J.G.S.M., S.P., and L.D.S. designed studies, interpreted results, and reviewed the manuscript. S.A.S. conceived and designed the studies, interpreted results, drafted, edited, and reviewed the manuscript.

Conflict of interest statement

S.A.S has received grant funding from Ono Pharmaceutical Co., Ltd. and is a consultant for Novo Nordisk.

REFERENCES

1. Walker, J. T., Saunders, D. C., Brissova, M. & Powers, A. C. The Human Islet: Mini-Organ With Mega-Impact. *Endocr. Rev.* **42**, 605–657 (2021).
2. Ramzy, A. *et al.* Implanted pluripotent stem-cell-derived pancreatic endoderm cells secrete glucose-responsive C-peptide in patients with type 1 diabetes. *Cell Stem Cell* **28**, 2047-2061.e5 (2021).
3. Reichman, T. W. *et al.* Stem Cell-Derived, Fully Differentiated Islets for Type 1 Diabetes. *N. Engl. J. Med.* (2025) doi:10.1056/NEJMoa2506549.
4. Hogrebe, N. J., Maxwell, K. G., Augsornworawat, P. & Millman, J. R. Generation of insulin-producing pancreatic β cells from multiple human stem cell lines. *Nat. Protoc.* **16**, 4109–4143 (2021).
5. Nair, G. G. *et al.* Recapitulating endocrine cell clustering in culture promotes maturation of human stem-cell-derived β cells. *Nat. Cell Biol.* **21**, 263–274 (2019).
6. Balboa, D. *et al.* Functional, metabolic and transcriptional maturation of human pancreatic islets derived from stem cells. *Nat. Biotechnol.* **40**, 1042–1055 (2022).
7. Liang, S. *et al.* Differentiation of stem cell-derived pancreatic progenitors into insulin-secreting islet clusters in a multiwell-based static 3D culture system. *Cell Rep. Methods* **3**, 100466 (2023).
8. Sui, L. *et al.* Reduced replication fork speed promotes pancreatic endocrine differentiation and controls graft size. *JCI Insight* **6**, e141553, 141553 (2021).
9. Barsby, T. *et al.* Aberrant metabolite trafficking and fuel sensitivity in human pluripotent stem cell-derived islets. *Cell Rep.* **42**, 112970 (2023).
10. Davis, J. C. *et al.* Glucose Response by Stem Cell-Derived β Cells In Vitro Is Inhibited by a Bottleneck in Glycolysis. *Cell Rep.* **31**, 107623 (2020).
11. Yoshihara, E. *et al.* ERRγ Is Required for the Metabolic Maturation of Therapeutically Functional Glucose-Responsive β Cells. *Cell Metab.* **23**, 622–634 (2016).

12. Augsornworawat, P., Maxwell, K. G., Velazco-Cruz, L. & Millman, J. R. Single-Cell Transcriptome Profiling Reveals β Cell Maturation in Stem Cell-Derived Islets after Transplantation. *Cell Rep.* **32**, 108067 (2020).

13. Picard, M. & Shirihai, O. S. Mitochondrial signal transduction. *Cell Metab.* **34**, 1620–1653 (2022).

14. Han, S. *et al.* Mitochondrial integrated stress response controls lung epithelial cell fate. *Nature* **620**, 890–897 (2023).

15. Ainscow, E. K., Zhao, C. & Rutter, G. A. Acute overexpression of lactate dehydrogenase-A perturbs beta-cell mitochondrial metabolism and insulin secretion. *Diabetes* **49**, 1149–1155 (2000).

16. Pullen, T. J. *et al.* Identification of genes selectively disallowed in the pancreatic islet. *Islets* **2**, 89–95 (2010).

17. Sasaki, M. *et al.* Reduction of reactive oxygen species ameliorates metabolism-secretion coupling in islets of diabetic GK rats by suppressing lactate overproduction. *Diabetes* **62**, 1996–2003 (2013).

18. Rutter, G. A., Georgiadou, E., Martinez-Sanchez, A. & Pullen, T. J. Metabolic and functional specialisations of the pancreatic beta cell: gene disallowance, mitochondrial metabolism and intercellular connectivity. *Diabetologia* **63**, 1990–1998 (2020).

19. Iworima, D. G. *et al.* Metabolic switching, growth kinetics and cell yields in the scalable manufacture of stem cell-derived insulin-producing cells. *Stem Cell Res. Ther.* **15**, 1 (2024).

20. Kamat, V. *et al.* A versatile pumpless multi-channel fluidics system for maintenance and real-time functional assessment of tissue and cells. *Cell Rep. Methods* **3**, 100642 (2023).

21. Lowell, B. B. & Shulman, G. I. Mitochondrial dysfunction and type 2 diabetes. *Science* **307**, 384–387 (2005).

22. Pinti, M. V. *et al.* Mitochondrial dysfunction in type 2 diabetes mellitus: an organ-based analysis. *Am. J. Physiol. Endocrinol. Metab.* **316**, E268–E285 (2019).

865 23. Sangwung, P., Petersen, K. F., Shulman, G. I. & Knowles, J. W. Mitochondrial
866 Dysfunction, Insulin Resistance, and Potential Genetic Implications. *Endocrinology* **161**,
867 bqaa017 (2020).
868 24. Pagliuca, F. W. *et al.* Generation of Functional Human Pancreatic β Cells In Vitro. *Cell*
869 **159**, 428–439 (2014).
870 25. Russ, H. A. *et al.* Controlled induction of human pancreatic progenitors produces
871 functional beta-like cells *in vitro*. *EMBO J.* **34**, 1759–1772 (2015).
872 26. Rath, S. *et al.* MitoCarta3.0: an updated mitochondrial proteome now with sub-organelle
873 localization and pathway annotations. *Nucleic Acids Res.* **49**, D1541–D1547 (2021).
874 27. Szklarczyk, D. *et al.* The STRING database in 2023: protein-protein association
875 networks and functional enrichment analyses for any sequenced genome of interest. *Nucleic*
876 *Acids Res.* **51**, D638–D646 (2023).
877 28. Augsornworawat, P. *et al.* Single-nucleus multi-omics of human stem cell-derived islets
878 identifies deficiencies in lineage specification. *Nat. Cell Biol.* **25**, 904–916 (2023).
879 29. Schmidt, M. D., Ishahak, M., Augsornworawat, P. & Millman, J. R. Comparative and
880 integrative single cell analysis reveals new insights into the transcriptional immaturity of stem
881 cell-derived β cells. *BMC Genomics* **25**, 105 (2024).
882 30. Prentki, M., Corkey, B. E. & Madiraju, S. R. M. Lipid-associated metabolic signalling
883 networks in pancreatic beta cell function. *Diabetologia* **63**, 10–20 (2020).
884 31. Imai, Y., Cousins, R. S., Liu, S., Phelps, B. M. & Promes, J. A. Connecting pancreatic
885 islet lipid metabolism with insulin secretion and the development of type 2 diabetes. *Ann. N.*
886 *Y. Acad. Sci.* **1461**, 53–72 (2020).
887 32. Schreurs, M., Kuipers, F. & van der Leij, F. R. Regulatory enzymes of mitochondrial beta-
888 oxidation as targets for treatment of the metabolic syndrome. *Obes. Rev. Off. J. Int. Assoc.*
889 *Study Obes.* **11**, 380–388 (2010).

890 33. Wang, Y. *et al.* Acetyl-CoA Carboxylases and Diseases. *Front. Oncol.* **12**, 836058
891 (2022).
892 34. Houten, S. M., Violante, S., Ventura, F. V. & Wanders, R. J. A. The Biochemistry and
893 Physiology of Mitochondrial Fatty Acid β-Oxidation and Its Genetic Disorders. *Annu. Rev.*
894 *Physiol.* **78**, 23–44 (2016).
895 35. Hai, Q. & Smith, J. D. Acyl-Coenzyme A: Cholesterol Acyltransferase (ACAT) in
896 Cholesterol Metabolism: From Its Discovery to Clinical Trials and the Genomics Era.
897 *Metabolites* **11**, 543 (2021).
898 36. Zammit, V. A., Ramsay, R. R., Bonomini, M. & Arduini, A. Carnitine, mitochondrial
899 function and therapy. *Adv. Drug Deliv. Rev.* **61**, 1353–1362 (2009).
900 37. Chen, E. Y. *et al.* Enrichr: interactive and collaborative HTML5 gene list enrichment
901 analysis tool. *BMC Bioinformatics* **14**, 128 (2013).
902 38. Kuleshov, M. V. *et al.* Enrichr: a comprehensive gene set enrichment analysis web
903 server 2016 update. *Nucleic Acids Res.* **44**, W90-97 (2016).
904 39. Xie, Z. *et al.* Gene Set Knowledge Discovery with Enrichr. *Curr. Protoc.* **1**, e90 (2021).
905 40. Brissova, M. *et al.* Reduction in pancreatic transcription factor PDX-1 impairs glucose-
906 stimulated insulin secretion. *J. Biol. Chem.* **277**, 11225–11232 (2002).
907 41. Gauthier, B. R. *et al.* PDX1 deficiency causes mitochondrial dysfunction and defective
908 insulin secretion through TFAM suppression. *Cell Metab.* **10**, 110–118 (2009).
909 42. Seale, P. *et al.* Transcriptional control of brown fat determination by PRDM16. *Cell*
910 *Metab.* **6**, 38–54 (2007).
911 43. Sugiyama, T. *et al.* Reconstituting pancreas development from purified progenitor cells
912 reveals genes essential for islet differentiation. *Proc. Natl. Acad. Sci. U. S. A.* **110**, 12691–
913 12696 (2013).
914 44. Fan, W. & Evans, R. PPARs and ERRs: molecular mediators of mitochondrial
915 metabolism. *Curr. Opin. Cell Biol.* **33**, 49–54 (2015).

916 45. Finck, B. N. & Kelly, D. P. PGC-1 coactivators: inducible regulators of energy metabolism
917 in health and disease. *J. Clin. Invest.* **116**, 615–622 (2006).
918 46. Handschin, C. & Spiegelman, B. M. Peroxisome Proliferator-Activated Receptor γ
919 Coactivator 1 Coactivators, Energy Homeostasis, and Metabolism. *Endocr. Rev.* **27**, 728–735
920 (2006).
921 47. Makowski, L. *et al.* Metabolic profiling of PPARalpha-/- mice reveals defects in carnitine
922 and amino acid homeostasis that are partially reversed by oral carnitine supplementation.
923 *FASEB J. Off. Publ. Fed. Am. Soc. Exp. Biol.* **23**, 586–604 (2009).
924 48. Wen, G., Ringseis, R., Rauer, C. & Eder, K. The mouse gene encoding the carnitine
925 biosynthetic enzyme 4-N-trimethylaminobutyraldehyde dehydrogenase is regulated by
926 peroxisome proliferator-activated receptor α. *Biochim. Biophys. Acta* **1819**, 357–365 (2012).
927 49. Tahri-Joutey, M. *et al.* Mechanisms Mediating the Regulation of Peroxisomal Fatty Acid
928 Beta-Oxidation by PPARα. *Int. J. Mol. Sci.* **22**, 8969 (2021).
929 50. Fang, L. *et al.* PPARgene: A Database of Experimentally Verified and Computationally
930 Predicted PPAR Target Genes. *PPAR Res.* **2016**, 1–6 (2016).
931 51. Schep, A. N., Wu, B., Buenrostro, J. D. & Greenleaf, W. J. chromVAR: inferring
932 transcription-factor-associated accessibility from single-cell epigenomic data. *Nat. Methods*
933 **14**, 975–978 (2017).
934 52. Gupta, D., Kono, T. & Evans-Molina, C. The role of peroxisome proliferator-activated
935 receptor γ in pancreatic β cell function and survival: therapeutic implications for the treatment
936 of type 2 diabetes mellitus. *Diabetes Obes. Metab.* **12**, 1036–1047 (2010).
937 53. Onodera, T. *et al.* Protective roles of adiponectin and molecular signatures of HNF4α
938 and PPARα as downstream targets of adiponectin in pancreatic β cells. *Mol. Metab.* **78**,
939 101821 (2023).
940 54. Lorberbaum, D. S. *et al.* Retinoic acid signaling within pancreatic endocrine progenitors
941 regulates mouse and human β cell specification. *Dev. Camb. Engl.* **147**, dev189977 (2020).

942 55. Capelli, D. *et al.* Structural basis for PPAR partial or full activation revealed by a novel
943 ligand binding mode. *Sci. Rep.* **6**, 34792 (2016).
944 56. Siclari, J. J. & Gardner, K. H. Two steps, one ligand: How PPARγ binds small-molecule
945 agonists. *Struct. Lond. Engl. 1993* **29**, 935–936 (2021).
946 57. Haakonsson, A. K., Stahl Madsen, M., Nielsen, R., Sandelin, A. & Mandrup, S. Acute
947 Genome-Wide Effects of Rosiglitazone on PPARγ Transcriptional Networks in Adipocytes.
948 *Mol. Endocrinol.* **27**, 1536–1549 (2013).
949 58. Kamata, S. *et al.* PPARα Ligand-Binding Domain Structures with Endogenous Fatty
950 Acids and Fibrates. *iScience* **23**, 101727 (2020).
951 59. Lin, Y., Wang, Y. & Li, P.-F. PPARα: An emerging target of metabolic syndrome,
952 neurodegenerative and cardiovascular diseases. *Front. Endocrinol.* **13**, 1074911 (2022).
953 60. Li, G. *et al.* Hepatic peroxisome proliferator-activated receptor alpha mediates the major
954 metabolic effects of Wy-14643. *J. Gastroenterol. Hepatol.* **33**, 1138–1145 (2018).
955 61. Wolf, D. C. *et al.* Comparative hepatic effects of perfluorooctanoic acid and WY 14,643
956 in PPAR-alpha knockout and wild-type mice. *Toxicol. Pathol.* **36**, 632–639 (2008).
957 62. Qiu, W.-L. *et al.* Deciphering Pancreatic Islet β Cell and α Cell Maturation Pathways and
958 Characteristic Features at the Single-Cell Level. *Cell Metab.* **27**, 702 (2018).
959 63. Bealer, E. *et al.* Extrahepatic transplantation of 3D cultured stem cell-derived islet
960 organoids on microporous scaffolds. *Biomater. Sci.* **11**, 3645–3655 (2023).
961 64. Li, F. *et al.* Fas Ligand-Modified Scaffolds Protect Stem Cell Derived β-Cells by
962 Modulating Immune Cell Numbers and Polarization. *ACS Appl. Mater. Interfaces* (2022)
963 doi:10.1021/acsami.2c12939.
964 65. Seale, P. Transcriptional Regulatory Circuits Controlling Brown Fat Development and
965 Activation. *Diabetes* **64**, 2369–2375 (2015).
966 66. Cheng, C.-F., Ku, H.-C. & Lin, H. PGC-1α as a Pivotal Factor in Lipid and Metabolic
967 Regulation. *Int. J. Mol. Sci.* **19**, 3447 (2018).

968 67. Shen, Y. *et al.* Shared PPARα/γ Target Genes Regulate Brown Adipocyte Thermogenic
969 Function. *Cell Rep.* **30**, 3079-3091.e5 (2020).
970 68. Cristancho, A. G. & Lazar, M. A. Forming functional fat: a growing understanding of
971 adipocyte differentiation. *Nat. Rev. Mol. Cell Biol.* **12**, 722–734 (2011).
972 69. Mao-Qiang, M. *et al.* Peroxisome-proliferator-activated receptor (PPAR)-gamma
973 activation stimulates keratinocyte differentiation. *J. Invest. Dermatol.* **123**, 305–312 (2004).
974 70. Hanley, K. *et al.* Keratinocyte differentiation is stimulated by activators of the nuclear
975 hormone receptor PPARalpha. *J. Invest. Dermatol.* **110**, 368–375 (1998).
976 71. Chougule, A. *et al.* Osteocytes contribute via nuclear receptor PPAR-alpha to
977 maintenance of bone and systemic energy metabolism. *Front. Endocrinol.* **14**, 1145467
978 (2023).
979 72. Lazarenko, O. P. *et al.* Rosiglitazone induces decreases in bone mass and strength that
980 are reminiscent of aged bone. *Endocrinology* **148**, 2669–2680 (2007).
981 73. Christofides, A., Konstantinidou, E., Jani, C. & Boussiotis, V. A. The role of peroxisome
982 proliferator-activated receptors (PPAR) in immune responses. *Metabolism.* **114**, 154338
983 (2021).
984 74. Lalloyer, F. *et al.* Peroxisome proliferator-activated receptor alpha improves pancreatic
985 adaptation to insulin resistance in obese mice and reduces lipotoxicity in human islets.
986 *Diabetes* **55**, 1605–1613 (2006).
987 75. Frigerio, F. *et al.* Peroxisome proliferator-activated receptor alpha (PPARalpha) protects
988 against oleate-induced INS-1E beta cell dysfunction by preserving carbohydrate metabolism.
989 *Diabetologia* **53**, 331–340 (2010).
990 76. Gastaldelli, A. *et al.* Thiazolidinediones improve β-cell function in type 2 diabetic patients.
991 *Am. J. Physiol.-Endocrinol. Metab.* **292**, E871–E883 (2007).
992 77. Kahn, S. E. *et al.* Glycemic durability of rosiglitazone, metformin, or glyburide
993 monotherapy. *N. Engl. J. Med.* **355**, 2427–2443 (2006).

994 78. Lupi, R. *et al.* Rosiglitazone prevents the impairment of human islet function induced by
995 fatty acids: evidence for a role of PPARgamma2 in the modulation of insulin secretion. *Am. J.*
996 *Physiol. Endocrinol. Metab.* **286**, E560-567 (2004).
997 79. Desmet, S. J. *et al. Crosstalk Interactions between Transcription Factors ERRα and*
998 *PPARα Assist PPARα-Mediated Gene Expression*.
999 http://biorxiv.org/lookup/doi/10.1101/2024.01.15.575655 (2024)
1000 doi:10.1101/2024.01.15.575655.
1001 80. Yu, D. D. & Forman, B. M. Identification of an agonist ligand for estrogen-related
1002 receptors ERRbeta/gamma. *Bioorg. Med. Chem. Lett.* **15**, 1311–1313 (2005).
1003 81. Wright, M. B., Bortolini, M., Tadayyon, M. & Bopst, M. Minireview: Challenges and
1004 opportunities in development of PPAR agonists. *Mol. Endocrinol. Baltim. Md* **28**, 1756–1768
1005 (2014).
1006 82. Botta, M. *et al.* PPAR Agonists and Metabolic Syndrome: An Established Role? *Int. J.*
1007 *Mol. Sci.* **19**, 1197 (2018).
1008 83. Gross, B., Pawlak, M., Lefebvre, P. & Staels, B. PPARs in obesity-induced T2DM,
1009 dyslipidaemia and NAFLD. *Nat. Rev. Endocrinol.* **13**, 36–49 (2017).
1010 84. Divakaruni, A. S. & Brand, M. D. The Regulation and Physiology of Mitochondrial Proton
1011 Leak. *Physiology* **26**, 192–205 (2011).
1012 85. Anwar, M., Kasper, A., Steck, A. R. & Schier, J. G. Bongkrekic Acid-a Review of a
1013 Lesser-Known Mitochondrial Toxin. *J. Med. Toxicol. Off. J. Am. Coll. Med. Toxicol.* **13**, 173–
1014 179 (2017).
1015 86. Ewart, R. B., Yousufzai, S. Y., Bradford, M. W. & Shrago, E. Rat islet mitochondrial
1016 adenine nucleotide translocase and the regulation of insulin secretion. *Diabetes* **32**, 793–797
1017 (1983).

1018 87. Kiranadi, B., Bangham, J. A. & Smith, P. A. Inhibition of electrical activity in mouse
1019 pancreatic beta-cells by the ATP/ADP translocase inhibitor, bongkrekic acid. *FEBS Lett.* **283**,
1020 93–96 (1991).
1021 88. Hua, H. *et al.* Remodeling ceramide homeostasis promotes functional maturation of
1022 human pluripotent stem cell-derived β cells. *Cell Stem Cell* S1934590924001371 (2024)
1023 doi:10.1016/j.stem.2024.04.010.
1024 89. Newgard, C. B. Interplay between lipids and branched-chain amino acids in
1025 development of insulin resistance. *Cell Metab.* **15**, 606–614 (2012).
1026 90. Helman, A. *et al.* A Nutrient-Sensing Transition at Birth Triggers Glucose-Responsive
1027 Insulin Secretion. *Cell Metab.* **31**, 1004-1016.e5 (2020).
1028 91. Innis, S. M. Polyunsaturated fatty acids in human milk: an essential role in infant
1029 development. *Adv. Exp. Med. Biol.* **554**, 27–43 (2004).
1030 92. Schupp, M. & Lazar, M. A. Endogenous ligands for nuclear receptors: digging deeper. *J.*
1031 *Biol. Chem.* **285**, 40409–40415 (2010).
1032 93. Grygiel-Górniak, B. Peroxisome proliferator-activated receptors and their ligands:
1033 nutritional and clinical implications--a review. *Nutr. J.* **13**, 17 (2014).
1034 94. Ramiro-Cortijo, D. *et al.* Breast Milk Lipids and Fatty Acids in Regulating Neonatal
1035 Intestinal Development and Protecting against Intestinal Injury. *Nutrients* **12**, 534 (2020).
1036 95. Pollinger, J. & Merk, D. Therapeutic applications of the versatile fatty acid mimetic
1037 WY14643. *Expert Opin. Ther. Pat.* **27**, 517–525 (2017).
1038 96. Wang, S. *et al.* Transplantation of chemically induced pluripotent stem-cell-derived islets
1039 under abdominal anterior rectus sheath in a type 1 diabetes patient. *Cell* **187**, 6152-6164.e18
1040 (2024).
1041 97. Hogrebe, N. J., Augsornworawat, P., Maxwell, K. G., Velazco-Cruz, L. & Millman, J. R.
1042 Targeting the cytoskeleton to direct pancreatic differentiation of human pluripotent stem cells.
1043 *Nat. Biotechnol.* **38**, 460–470 (2020).

1044 98. Baek, J. *et al.* The deacylase sirtuin 5 reduces malonylation in nonmitochondrial
1045 metabolic pathways in diabetic kidney disease. *J. Biol. Chem.* **299**, 102960 (2023).
1046 99. Sas, K. M. *et al.* Tissue-specific metabolic reprogramming drives nutrient flux in diabetic
1047 complications. *JCI Insight* **1**, e86976 (2016).
1048 100. Belmonte, F. R. *et al.* Digital PCR methods improve detection sensitivity and
1049 measurement precision of low abundance mtDNA deletions. *Sci. Rep.* **6**, 25186 (2016).
1050 101. Karamanlidis, G. *et al.* Defective DNA replication impairs mitochondrial biogenesis in
1051 human failing hearts. *Circ. Res.* **106**, 1541–1548 (2010).
1052 102. Sidarala, V. *et al.* Mitofusin 1 and 2 regulation of mitochondrial DNA content is a critical
1053 determinant of glucose homeostasis. *Nat. Commun.* **13**, 2340 (2022).
1054 103. Zhang, Y., Parmigiani, G. & Johnson, W. E. ComBat-seq: batch effect adjustment for
1055 RNA-seq count data. *NAR Genomics Bioinforma.* **2**, lqaa078 (2020).
1056 104. Leek, J. T., Johnson, W. E., Parker, H. S., Jaffe, A. E. & Storey, J. D. The sva package
1057 for removing batch effects and other unwanted variation in high-throughput experiments.
1058 *Bioinforma. Oxf. Engl.* **28**, 882–883 (2012).
1059 105. Moon, K. R. *et al.* Visualizing structure and transitions in high-dimensional biological
1060 data. *Nat. Biotechnol.* **37**, 1482–1492 (2019).
1061 106. Korsunsky, I. *et al.* Fast, sensitive and accurate integration of single-cell data with
1062 Harmony. *Nat. Methods* **16**, 1289–1296 (2019).
1063 107. Zhang, Y. *et al.* Model-based Analysis of ChIP-Seq (MACS). *Genome Biol.* **9**, R137
1064 (2008).
1065 108. Stuart, T., Srivastava, A., Madad, S., Lareau, C. A. & Satija, R. Single-cell chromatin
1066 state analysis with Signac. *Nat. Methods* **18**, 1333–1341 (2021).
1067 109. Rauluseviciute, I. *et al.* JASPAR 2024: 20th anniversary of the open-access database of
1068 transcription factor binding profiles. *Nucleic Acids Res.* **52**, D174–D182 (2024).

110. Chaudhry, A., Shi, R. & Luciani, D. S. A pipeline for multidimensional confocal analysis of mitochondrial morphology, function, and dynamics in pancreatic β-cells. *Am. J. Physiol. Endocrinol. Metab.* **318**, E87–E101 (2020).

111. Motulsky, H. J. & Brown, R. E. Detecting outliers when fitting data with nonlinear regression - a new method based on robust nonlinear regression and the false discovery rate. *BMC Bioinformatics* **7**, 123 (2006).

1080 **FIGURE LEGENDS**

1081 **Figure 1. SC-islets are transcriptionally and metabolically immature.** (A) A schematic
1082 diagram illustrating the cell stages during differentiation of human pluripotent stem cells (hPSCs)
1083 into SC-islets. (B) Differential RNA expression heatmap, displayed as integrated mean $\log_2$ fold
1084 change (FC), from RNA-seq data of representative stage marker expression at each
1085 differentiation stage (*n* = 4-5 differentiations or independent human islet donors/group). (C)
1086 Immunofluorescence images at 60X magnification of stage 6 SC-islets for C-peptide (green),
1087 Glucagon (red), Somatostatin (red), and DAPI (blue) (*n* = 3/group). Scale bars, 20 μm. (D)
1088 Differential RNA expression heatmap of genes encoding islet cell maturation markers and
1089 hormones in stage 6 SC-islets (*n* = 5) and non-diabetic human islet donors (*n* = 6). FC is relative
1090 to the average across all individual samples. (E) Insulin secretion following static incubations in
1091 1.67 mM glucose (1.67G), 16.7 mM glucose (16.7G), and 30 mM KCl (30 KCl) normalized to
1092 insulin content in stage 6 SC-islets and human islets (*n* = 3 differentiations or independent human
1093 islet donors/group); $^*P < 0.05$, $^{**}P < 0.01$ by two-way ANOVA followed by Tukey's multiple
1094 comparisons test. (F) Islet total insulin content normalized to protein content in stage 6 SC-islets
1095 and human islets (*n* = 5 differentiations and 4 independent human islet donors/group); $^*P < 0.05$
1096 unpaired *t*-test. Differential metabolomics heatmap demonstrating mean content of pyruvate (G)
1097 or lactate (H) at 5 mM glucose (5G) and 20 mM glucose (20G) for differentiation stages 1 through
1098 6 (*n* = 3/group) and human islets (*n* = 5 independent islet donors). (I) Oxygen consumption rate
1099 (OCR) fractional change in stage 6 SC-islets (*n* = 4 differentiations) and human islets (*n* = 5
1100 independent islet donors) following exposure to 2 mM glucose (2G), 20 mM glucose (20G), 10
1101 μM oligomycin, 1 μM FCCP, and 3 mM KCN. Data are presented as mean from independent
1102 differentiations or donors ± SEM; $^*P < 0.05$, $^{**}P < 0.01$ by unpaired *t*-test of fractional OCR value
1103 at designated time point for minimal or maximal respiration by oligomycin or FCCP, respectively.

1104

1105 **Figure 2. SC-islets display comparable mitochondrial DNA content, mass, and architecture**
1106 **to human islets.** (A) Quantification of ratio of mitochondrial DNA to nuclear DNA by qPCR for
1107 stage 0-6 cells and human islets (*n* = 4/group). (B) Quantification of single strand mitochondrial
1108 DNA products measured by qPCR for stage 0-6 cells and human islets (*n* = 3-4/group). (C)
1109 Quantification of citrate synthase activity normalized to total protein content for stage 0-6 cells
1110 and human islets (*n* = 3-4/group). (D) Representative Western blot (WB) of TOM20 protein
1111 expression for stage 0-6 cells and two different human islet donors (left). Vinculin serves as a
1112 loading control. Quantification (right) of TOM20 expression (normalized to Vinculin expression)
1113 via densitometry of the Western blots (*n* = 4-5/group). (E) Representative transmission electron
1114 microscopy (TEM) images of stage 6 SC-β cells and primary human β cells (left) and quantification
1115 of mitochondria ultrastructure (right) (*n* = 3/group, ~150 β cell mitochondria scored/sample).
1116
1117 **Figure 3. Transcriptomic profiling of SC-islets versus human islets reveals potential**
1118 **limitations in mitochondrial metabolism.** (A) Volcano plot depicting differential RNA expression
1119 in stage 6 SC-islets compared to human islets (*n* = 6 differentiations or independent human islet
1120 donors/group). Significantly differentially expressed genes demarcated by -FDR > 0.5 and |FC| >
1121 1.4. MitoCarta 3.0 genes are highlighted in purple. (B) Differential RNA expression heatmaps from
1122 RNA-seq data demonstrating expression of significantly differentially expressed MitoCarta 3.0
1123 genes in stage 0-6 cells compared to human islets (*n* = 4-6 differentiations or independent human
1124 islet donors/group). FC is relative to the average across all individual samples. Selected terms
1125 from Enrichr analysis of differentially expressed MitoCarta genes from stage 6 SC-islets vs.
1126 human islets analyzed with the following libraries: (C) WikiPathway 2023 Human and (D) KEGG
1127 2021 Human. (E) STRING analysis of MitoCarta genes with reduced expression in stage 6 SC-
1128 islets compared to human islets.
1129

1130 **Figure 4. Reduced expression of the OXPHOS machinery in SC-islets. (**A) Differential RNA
1131 expression heatmap, displayed as integrated mean $\log_2$ fold change (FC), from RNA-seq data of
1132 genes related to glucose transport and glycolysis at each differentiation stage and human islets
1133 (*n* = 4-5 differentiations or independent human islet donors/group). (B) Differential RNA
1134 expression heatmap (presented as integrated mean/group) of genes encoding OXPHOS
1135 components at each differentiation stage as well as human islet donors (*n* = 4-6/group). (C)
1136 Differential RNA expression heatmaps from RNAseq demonstrating expression of OXPHOS
1137 machinery genes in stage 0-6 cells and human islets (*n* = 4-6 differentiations or independent
1138 human islet donors/group). FC is relative to the average across all individual samples. (D)
1139 Differential RNA expression heatmap, displayed as integrated mean $\log_2$FC, from scRNA-seq of
1140 genes related to glycolysis and glucose transport and OXPHOS between SC-β cells to primary β
1141 cells as well as OXPHOS genes between SC-α cells to primary α cells. Data curated from
1142 Augsornworawat *et al*.[28]. (E) Representative Western blot analysis of expression of OXPHOS
1143 subunits, including ATP5A (Complex V), UQCRC2 (Complex III), NDUFA9 (Complex I), SDHB
1144 (Complex II), and COXII (Complex IV) in stage 0-6 cells and human islets (left). Vinculin serves
1145 as a loading control. Quantification (right) of ATP5A, UQCRC2, NDUFA9, SDHB, and COXII
1146 protein expression by densitometry (normalized for Vinculin expression) of the Western blots of
1147 stage 0-6 cells and human islets (*n* = 4 differentiations or independent human islet donors/group);
1148 $^{*}P < 0.05$, $^{**}P < 0.01$, $^{***}P < 0.001$, by one-way ANOVA followed by Dunnett's multiple
1149 comparisons test.
1150
1151 **Figure 5. Limitations in mitochondrial lipid metabolism in SC-islets.** Differential RNA
1152 expression heatmaps from RNA-seq data demonstrating expression of fatty acid biosynthesis (A)
1153 or fatty acid β-oxidation (B) genes in stage 0-6 cells and human islets (*n* = 4-6 differentiations or
1154 independent human islet donors/group). FC is relative to the average across all individual
1155 samples. (C) Differential RNA expression heatmaps from RNA-seq data demonstrating

1156 expression of lipid metabolism genes in stage 0-6 cells and human islets (*n* = 3-5 differentiations
1157 or independent human islet donors/group). FC is relative to the average across all individual
1158 samples. Lipidomics profiling of (D) L-carnitine (E) and short- or long-chain acylcarnitines
1159 (normalized to protein content) for stage 1-6 cells (*n* = 3/group) and human islets (*n* = 4-5
1160 independent islet donors); *$P < 0.05$, **$P < 0.01$, ****$P < 0.0001$ by one-way ANOVA followed by
1161 Dunnett's multiple comparisons test. (F) Differential RNA expression heatmaps from RNA-seq
1162 data demonstrating expression of expression of carnitine biosynthesis and short- and medium-
1163 chain acylcarnitine synthesis genes in stage 0-6 cells and human islets (*n* = 3-5 differentiations
1164 or independent human islet donors/group). FC is relative to the average across all individual
1165 samples.
1166
1167 **Figure 6. SC-islets display reduced expression of PPARα and PPARγ transcriptional**
1168 **targets.** Enrichr analysis of significantly differentially expressed genes from stage 6 SC-islets
1169 compared to human islets analyzed with the following libraries: (A) ChEA 2022 and (B)
1170 Transcription factor (TF) perturbations followed by expression. (C) Differential RNA expression
1171 heatmap from RNA-seq data demonstrating integrated mean expression of PPARα targets for
1172 stage 6 SC-islets and human islets (*n* = 6/group). (D) Differential RNA expression heatmap from
1173 RNA-seq data demonstrating integrated mean expression of genes encoding components of the
1174 PPAR-RXR transcriptional binding complex, including transcriptional co-activators, in stage 6 SC-
1175 islets and human islets (*n* = 6/group). (E) Representative Western blot analysis of expression of
1176 PPARα in stage 0-6 cells and human islets (left). Vinculin serves as a loading control.
1177 Quantification (right) of PPARα protein expression by densitometry (normalized to Vinculin
1178 expression) of the Western blots of stage 0-6 cells and human islets (*n* = 3 differentiations or 4
1179 independent human islet donors/group); *$P < 0.05$ by one-way ANOVA followed by Dunnett's
1180 multiple comparisons test. (F) Differential RNA expression heatmap generated from publicly-
1181 available scRNA-seq data[28] demonstrating integrated mean expression of genes encoding

1182 components of the PPAR-RXR transcriptional binding complex, including transcriptional co-
1183 activators, in SC-β cells and primary β cells. (G) Differential chromatin accessibility heatmap
1184 generated from publicly-available scATACseq data[28] demonstrating integrated mean motif
1185 accessibility of PPAR and RXR binding sites in SC-β cells and primary β cells. (H) Minimum to
1186 maximum box and whisker plots of normalized expression of *PPARA* across SC-β cells
1187 differentiation trajectory and primary β cells generated from publicly-available scRNA-seq data[28]
1188 (*n* = 3-4 differentiations or independent human islet donors/group). (I) Minimum to maximum box
1189 and whisker plots of PPARA module scores across SC-β cells differentiation trajectory and primary
1190 β cells generated from publicly-available scRNA-seq data[28] representing PPARA target gene
1191 expression (*n* = 3-4 differentiations or independent human islet donors/group). (J) Minimum to
1192 maximum box and whisker plots of motif deviation z-scored across SC-β cells differentiation
1193 trajectory and primary β cells generated from publicly-available scATAC-seq data[28] representing
1194 PPARα motif activity (*n* = 3-4 differentiations or independent human islet donors/group).
1195
1196 **Figure 7. WY14643 promotes the formation of SC-β cells.** (A) A schematic diagram illustrating
1197 use of the PPARα agonist WY14643 within the differentiation protocol. (B) Immunofluorescence
1198 images at 60X magnification (left) of vehicle control and WY14643-treated stage 6 SC-islets for
1199 C-peptide (green), glucagon (red), and DAPI (DNA - blue) or C-peptide (green), somatostatin
1200 (red), and DAPI (DNA - blue) (*n* = 3/group). Scale bars, 20 μm. Quantification (right) of C-peptide
1201 positive cells, dual hormone-positive cells, either C-peptide and glucagon (GCG) dual-positive or
1202 C-peptide and somatostatin (SST) dual-positive, as well as GCG-positive cells, and SST-positive
1203 cells (*n* = 3 differentiations/group, ~1000 cells quantified/differentiation and respective condition);
1204 ***$P < 0.001$ by unpaired Student's *t*-test. (C) Immunofluorescence images at 20X magnification
1205 (left) of vehicle control and WY14643-treated stage 6 SC-islets for C-peptide (green) and NKX6.1
1206 (red) (*n* = 3/group). Scale bars, 50 μm. Quantification (right) of the fractional change of NKX6.1/C-
1207 peptide co-positive cells per high powered field (*n* = 12-15 fields quantified/group, ~1000 cells

1208 quantified/differentiation and respective condition from 3 differentiations/group); $^{**}P < 0.01$ by
1209 unpaired Student's *t*-test. (D) Immunofluorescence images at 20X magnification (left) of vehicle
1210 control and WY14643-treated stage 6 SC-islets for C-peptide (green) and PDX1 (red) (n =
1211 3/group). Scale bars, 50 μm. Quantification (right) of the fractional change of PDX1/C-peptide co-
1212 positive cells per high powered field (n = 12-15 fields quantified/group, ~1000 cells
1213 quantified/differentiation and respective condition from 3 differentiations/group). (E) Differential
1214 RNA expression heatmap (presented as integrated mean/group) of PPARα targets for vehicle
1215 control and WY14643-treated stage 6 SC-islets (n = 4/group). (F) Differential RNA expression
1216 heatmap (presented as integrated mean/group) of mature β cell markers for vehicle control and
1217 WY14643-treated stage 6 SC-islets (n = 4/group). (G) Differential RNA expression heatmap
1218 (presented as integrated mean/group) of immature β cell markers for vehicle control and
1219 WY14643-treated stage 6 SC-islets (n = 4/group). (H) Differential RNA expression heatmap
1220 (presented as integrated mean/group) of genes encoding OXPHOS components for vehicle
1221 control and WY14643-treated stage 6 SC-islets (n = 4/group). (I) Differential RNA expression
1222 heatmap (presented as integrated mean/group) of genes encoding glucose transporters and
1223 glycolytic enzymes for vehicle control and WY14643-treated stage 6 SC-islets (n = 4/group). (J)
1224 Insulin secretion (left) with insulin stimulation index (right) following static incubations in 1.67 mM
1225 glucose (1.67G), 16.7 mM glucose (16.7G) and 30 mM KCl (30KCl) normalized to insulin content
1226 in vehicle control and WY14643-treated stage 6 SC-islets (n = 4 differentiations/group); $^{**}P < 0.01$
1227 by two-way ANOVA. (K) Oxygen consumption rate (OCR) fractional change in vehicle control and
1228 WY14643-treated stage 6 SC-islets (n = 3 differentiations) following exposure to 2 mM glucose
1229 (2G), 20 mM glucose (20G), 10 μM oligomycin, 1 μM FCCP, and 3 mM KCN. Data are presented
1230 as mean from independent differentiations ± SEM; $P = 0.057$ by ANOVA of fractional OCR value
1231 at designated time points following 20 mM glucose exposure. (L) Representative Western blot
1232 analysis of NDUFA9 protein expression for vehicle control and WY14643-treated stage 6 SC-
1233 islets (left). Vinculin serves as a loading control. Quantification (right) of NDUFA9 expression

1234 (normalized to Vinculin expression) via densitometry of the Western blots (n = 4/group); *P < 0.05
1235 by unpaired Student's t-test.
1236
1237 **Figure 8. Formation of SC-β cells by WY14643 is durable *in vivo* following transplantation.**
1238 (A) A schematic diagram illustrating the addition of WY14643 to the differentiation protocol,
1239 seeding of SC-islets onto poly(lactide-*co*-glycolide) (PLG) microporous scaffolds, and scaffold
1240 transplantation into NSG mice. (B) Immunofluorescence images at 20X and 60X magnification of
1241 stage 6 SC-islets for C-peptide (green), human nuclear antigen (red), and DAPI (blue) (n =
1242 3/group). Human nuclear antigen was used to distinguish human transplanted cells from murine
1243 recipient cells in the inguinal fat pad. Scale bars, 20 μm. (C) Immunofluorescence images at 60X
1244 magnification of vehicle control and WY14643-treated stage 6 SC-islets in explanted scaffold from
1245 NSG mice 10 days post-transplant for C-peptide (green), glucagon (red), and DAPI (blue) or C-
1246 peptide (green), somatostatin (red), and DAPI (blue) (n = 3-4/group). Scale bars = 20 μm. (D)
1247 Quantification of C-peptide-positive cells only, dual hormone-positive cells, both C-peptide- and
1248 GCG- or SST-positive cells, GCG-positive cells, and SST-positive cells by immunostaining in
1249 vehicle control and WY14643-treated stage 6 SC-islets in explanted scaffold from NSG mice 10
1250 days post-transplant (n = 3-4/group); *P < 0.05 by unpaired Student's t-test. (E) Insulin content
1251 normalized to total protein content for vehicle control and WY14643-treated explanted scaffolds
1252 from NSG mice 10 days post-transplant (n = 3-4/group); *P < 0.05 by unpaired Student's t-test.
1253 (F) Quantification of Ki-67 and C-peptide co-positive cells by immunostaining in vehicle control
1254 and WY14643-treated stage 6 SC-islets in explanted scaffold from NSG mice 10 days post-
1255 transplant (n = 4/group). (G) Immunofluorescence images (right) at 60X magnification of vehicle
1256 control and WY14643-treated stage 6 SC-islets in explanted scaffold from NSG mice 10 days
1257 post-transplant for C-peptide (green), OXPHOS (red), and DAPI (blue) (n = 3-4/group). Scale
1258 bars, 20 μm. Quantification (right) of mitochondrial morphology and networking utilizing
1259 Mitochondria Analyzer (n = 3-4/group, ~150 cells analyzed per differentiation and treatment).

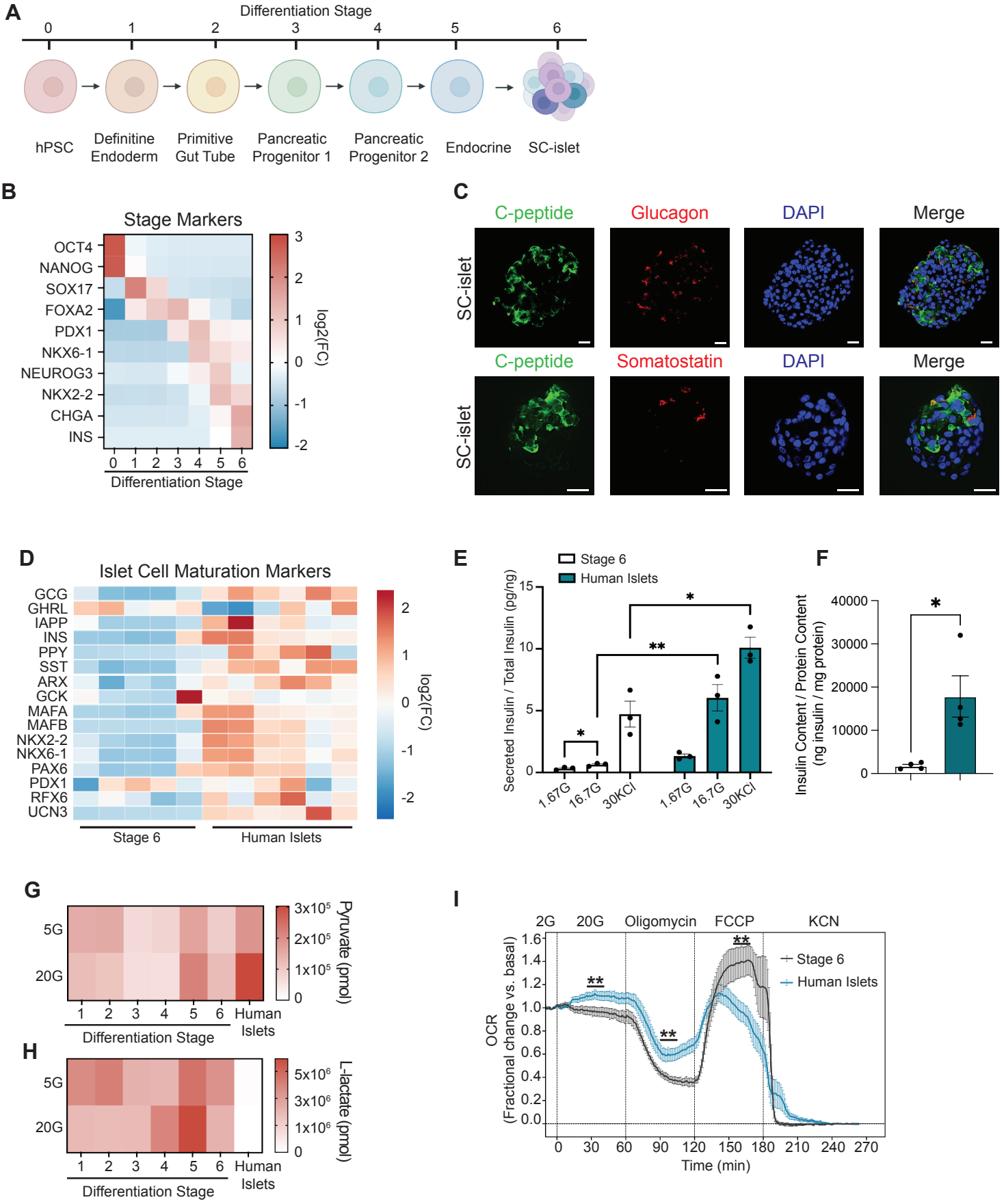
A
Differentiation Stage
0
1
2
3
4
5
6
hPSC
Definitive Endoderm
Primitive Gut Tube
Pancreatic Progenitor 1
Pancreatic Progenitor 2
Endocrine
SC-islet
B
Stage Markers
OCT4
NANOG
SOX17
FOXA2
PDX1
NKX6-1
NEUROG3
NKX2-2
CHGA
INS
Differentiation Stage
log2(FC)
C
C-peptide
Glucagon
DAPI
Merge
SC-islet
C-peptide
Somatostatin
DAPI
Merge
SC-islet
D
Islet Cell Maturation Markers
GCG
GHRL
IAPP
INS
PPY
SST
ARX
GCK
MAFA
MAFB
NKX2-2
NKX6-1
PAX6
PDX1
RFX6
UCN3
Stage 6
Human Islets
log2(FC)
E
Stage 6
Human Islets
Secreted Insulin / Total Insulin (pg/ng)
1.67G
16.7G
30KCl
F
Insulin Content / Protein Content (ng insulin / mg protein)
G
5G
20G
Pyruvate (pmol)
Human Islets
Differentiation Stage
H
5G
20G
L-lactate (pmol)
Human Islets
Differentiation Stage
I
2G
20G
Oligomycin
FCCP
KCN
Stage 6
Human Islets
OCR (Fractional change vs. basal)
Time (min)

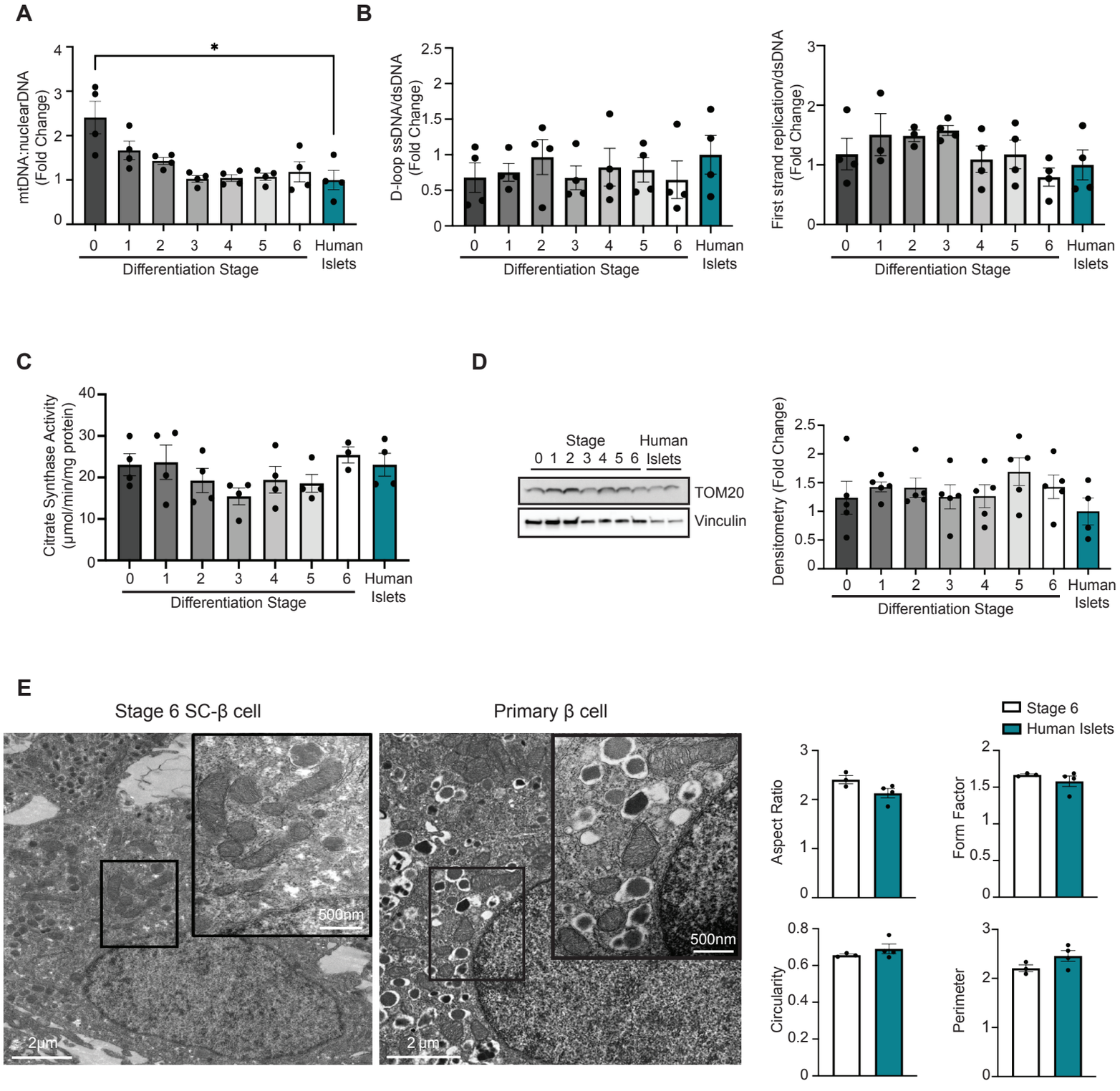
A
mtDNA:nuclearDNA (Fold Change)
*
0 1 2 3 4 5 6 Human Islets
Differentiation Stage
B
D-loop ssDNA/dsDNA (Fold Change)
First strand replication/dsDNA (Fold Change)
C
Citrate Synthase Activity (µmol/min/mg protein)
D
Stage
Human Islets
TOM20
Vinculin
Densitometry (Fold Change)
E
Stage 6 SC-β cell
Primary β cell
500nm
2µm
Stage 6
Human Islets
Aspect Ratio
Form Factor
Circularity
Perimeter

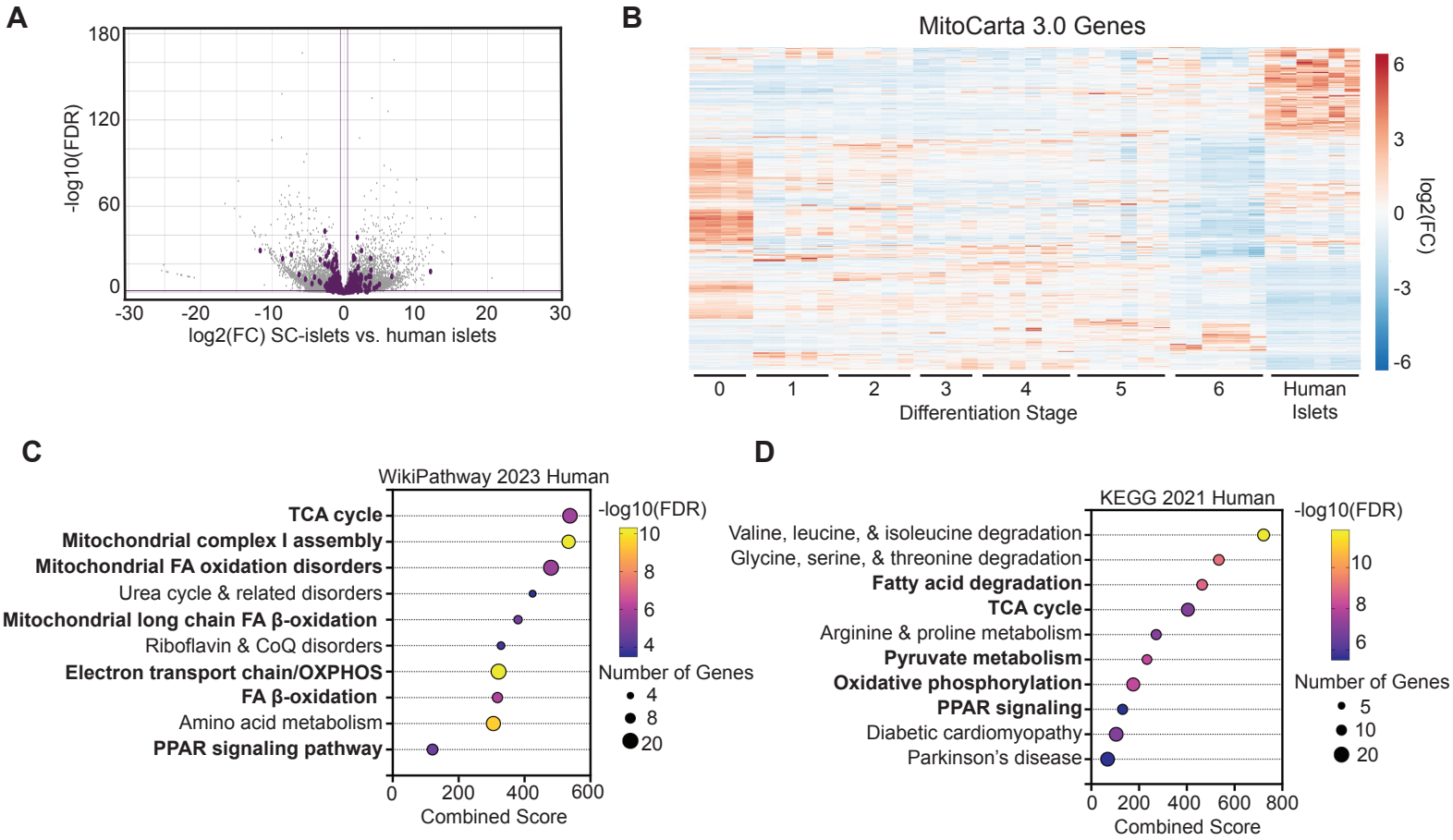

E

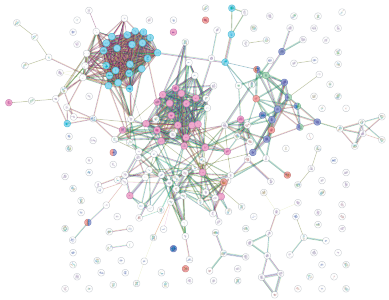

Biologic Process (Gene Ontology)	FDR
Mitochondrial Translation (GO:0032543)	1.83E-18
Oxidative Phosphorylation (GO:0006119)	9.11E-18
Cellular Lipid Catabolic Process (GO:0044242)	1.50E-05
Fatty Acid Biosynthetic Process (GO:0006633)	5.40E-03
Carnitine Metabolic Process (GO:0009437)	6.10E-03

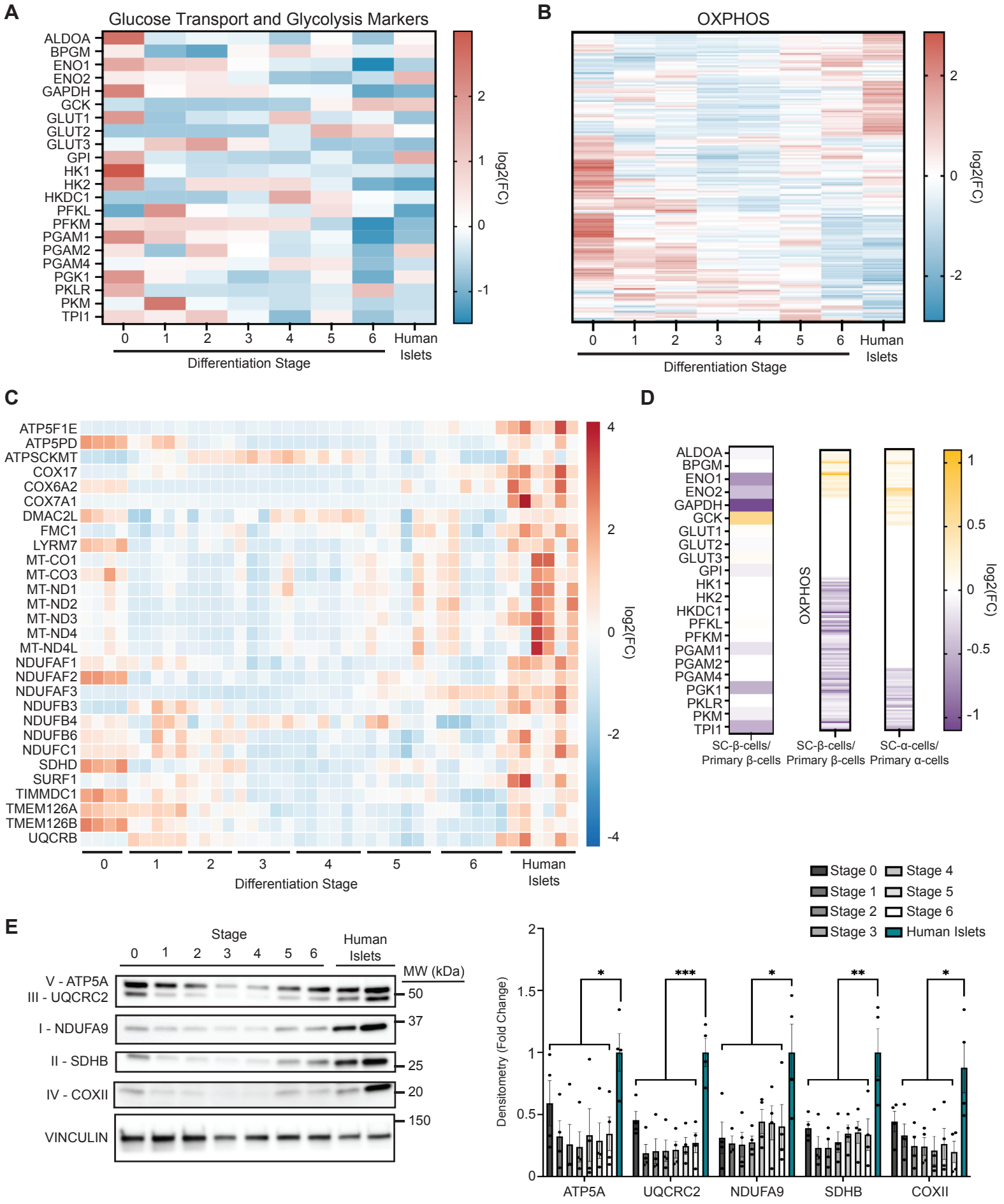
A
Glucose Transport and Glycolysis Markers
ALDOA
BPGM
ENO1
ENO2
GAPDH
GCK
GLUT1
GLUT2
GLUT3
GPI
HK1
HK2
HKDC1
PFKL
PFKM
PGAM1
PGAM2
PGAM4
PGK1
PKLR
PKM
TPI1
0 1 2 3 4 5 6 Human Islets
Differentiation Stage
log2(FC)
B
OXPHOS
Differentiation Stage
C
ATP5F1E
ATP5PD
ATPSCKMT
COX17
COX6A2
COX7A1
DMAC2L
FMC1
LYRM7
MT-CO1
MT-CO3
MT-ND1
MT-ND2
MT-ND3
MT-ND4
MT-ND4L
NDUFAF1
NDUFAF2
NDUFAF3
NDUFB3
NDUFB4
NDUFB6
NDUFC1
SDHD
SURF1
TIMMDC1
TMEM126A
TMEM126B
UQCRB
Differentiation Stage
D
OXPHOS
SC-β-cells/ Primary β-cells
SC-β-cells/ Primary β-cells
SC-α-cells/ Primary α-cells
E
Stage
Human Islets
MW (kDa)
V - ATP5A
III - UQCRC2
I - NDUFA9
II - SDHB
IV - COXII
VINCULIN
50
37
25
20
150
Stage 0
Stage 1
Stage 2
Stage 3
Stage 4
Stage 5
Stage 6
Human Islets
Densitometry (Fold Change)
ATP5A
UQCRC2
NDUFA9
SDHB
COXII

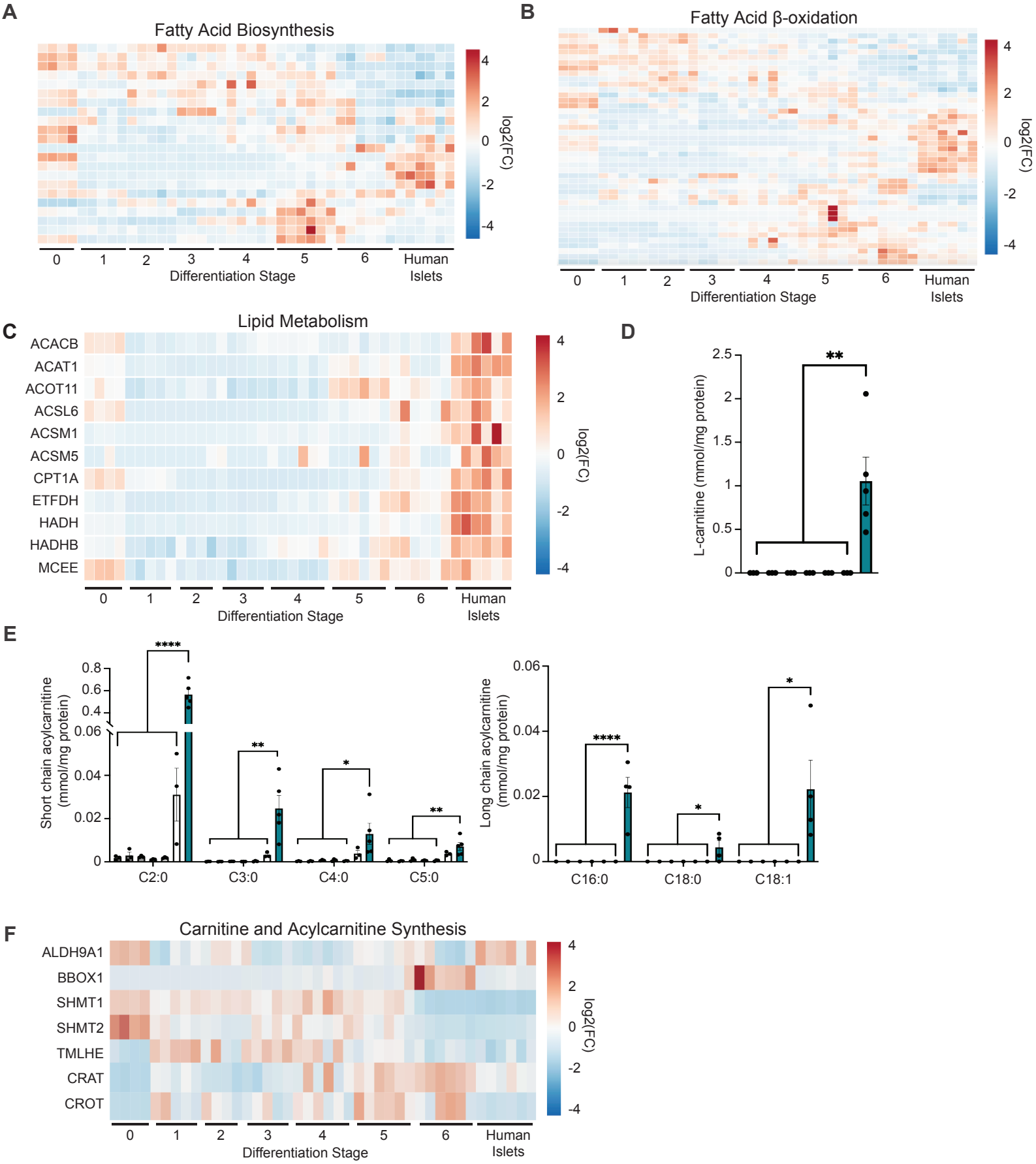
A
Fatty Acid Biosynthesis
log2(FC)
4
2
0
-2
-4
0
1
2
3
4
5
6
Human Islets
Differentiation Stage
B
Fatty Acid β-oxidation
log2(FC)
4
2
0
-2
-4
0
1
2
3
4
5
6
Human Islets
Differentiation Stage
C
Lipid Metabolism
ACACB
ACAT1
ACOT11
ACSL6
ACSM1
ACSM5
CPT1A
ETFDH
HADH
HADHB
MCEE
log2(FC)
4
2
0
-2
-4
0
1
2
3
4
5
6
Human Islets
Differentiation Stage
D
L-carnitine (mmol/mg protein)
2.5
2
1.5
1
0.5
0
**
E
Short chain acylcarnitine (mmol/mg protein)
0.8
0.6
0.4
0.06
0.04
0.02
0
****
**
*
**
C2:0
C3:0
C4:0
C5:0
Long chain acylcarnitine (mmol/mg protein)
0.06
0.04
0.02
0
****
*
*
C16:0
C18:0
C18:1
F
Carnitine and Acylcarnitine Synthesis
ALDH9A1
BBOX1
SHMT1
SHMT2
TMLHE
CRAT
CROT
log2(FC)
4
2
0
-2
-4
0
1
2
3
4
5
6
Human Islets
Differentiation Stage

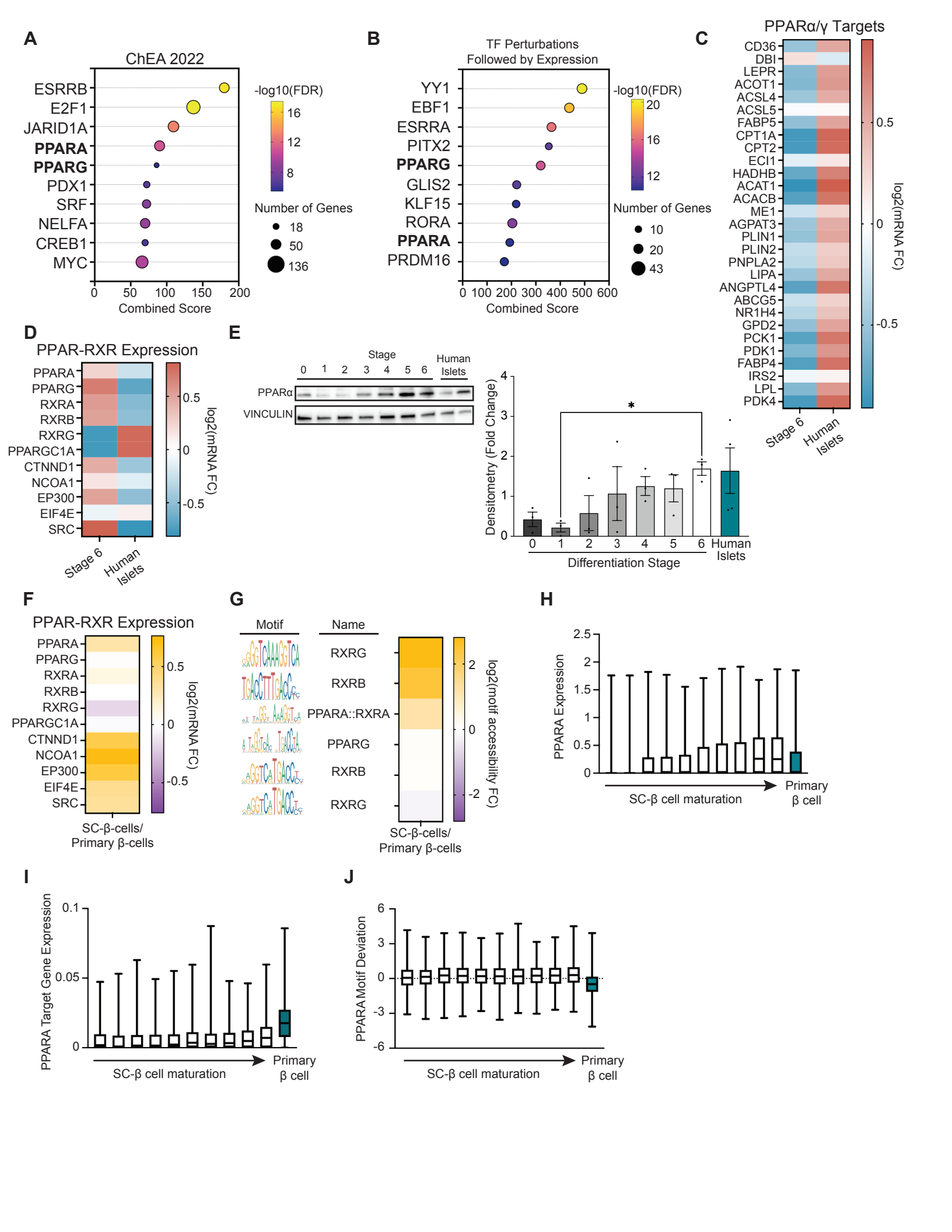
A
ChEA 2022
ESRRB
E2F1
JARID1A
PPARA
PPARG
PDX1
SRF
NELFA
CREB1
MYC
0 50 100 150 200
Combined Score
-log10(FDR)
16
12
8
Number of Genes
18
50
136
B
TF Perturbations
Followed by Expression
YY1
EBF1
ESRRA
PITX2
PPARG
GLIS2
KLF15
RORA
PPARA
PRDM16
0 100 200 300 400 500 600
Combined Score
-log10(FDR)
20
16
12
Number of Genes
10
20
43
C
PPARα/γ Targets
CD36
DBI
LEPR
ACOT1
ACSL4
ACSL5
FABP5
CPT1A
CPT2
ECI1
HADHB
ACAT1
ACACB
ME1
AGPAT3
PLIN1
PLIN2
PNPLA2
LIPA
ANGPTL4
ABCG5
NR1H4
GPD2
PCK1
PDK1
FABP4
IRS2
LPL
PDK4
Stage 6
Human Islets
log2(mRNA FC)
0.5
0
-0.5
D
PPAR-RXR Expression
PPARA
PPARG
RXRA
RXRB
RXRG
PPARGC1A
CTNND1
NCOA1
EP300
EIF4E
SRC
Stage 6
Human Islets
log2(mRNA FC)
0.5
0
-0.5
E
Stage
0 1 2 3 4 5 6
Human Islets
PPARα
VINCULIN
Densitometry (Fold Change)
0 1 2 3 4
*
0 1 2 3 4 5 6 Human Islets
Differentiation Stage
F
PPAR-RXR Expression
PPARA
PPARG
RXRA
RXRB
RXRG
PPARGC1A
CTNND1
NCOA1
EP300
EIF4E
SRC
SC-β-cells/
Primary β-cells
log2(mRNA FC)
0.5
0
-0.5
G
Motif
Name
RXRG
RXRB
PPARA::RXRA
PPARG
RXRB
RXRG
SC-β-cells/
Primary β-cells
log2(motif accessibility FC)
2
0
-2
H
PPARA Expression
0 0.5 1 1.5 2 2.5
SC-β cell maturation
Primary β cell
I
PPARA Target Gene Expression
0 0.05 0.1
SC-β cell maturation
Primary β cell
J
PPARA Motif Deviation
-6 -3 0 3 6
SC-β cell maturation
Primary β cell

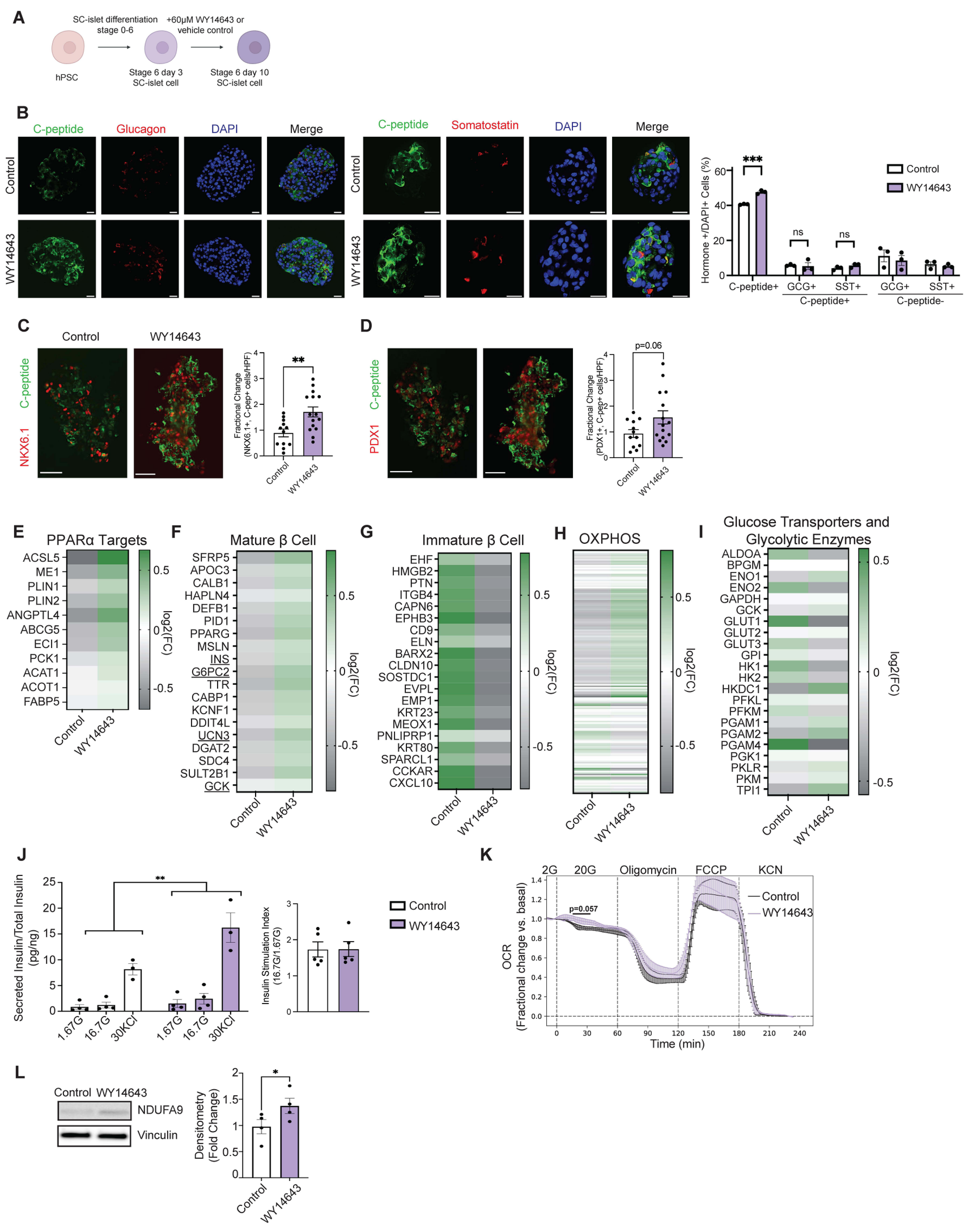
A
SC-islet differentiation stage 0-6
+60μM WY14643 or vehicle control
hPSC
Stage 6 day 3 SC-islet cell
Stage 6 day 10 SC-islet cell
B
C-peptide
Glucagon
DAPI
Merge
Control
WY14643
C-peptide
Somatostatin
DAPI
Merge
Control
WY14643
Hormone +/DAPI+ Cells (%)
***
ns
ns
Control
WY14643
C-peptide+
GCG+
SST+
C-peptide+
GCG+
SST+
C-peptide-
C
Control
WY14643
C-peptide
NKX6.1
Fractional Change (NKX6.1+, C-pep+ cells/HPF)
**
Control
WY14643
D
C-peptide
PDX1
Fractional Change (PDX1+, C-pep+ cells/HPF)
p=0.06
Control
WY14643
E
PPARα Targets
ACSL5
ME1
PLIN1
PLIN2
ANGPTL4
ABCG5
ECI1
PCK1
ACAT1
ACOT1
FABP5
log2(FC)
Control
WY14643
F
Mature β Cell
SFRP5
APOC3
CALB1
HAPLN4
DEFB1
PID1
PPARG
MSLN
INS
G6PC2
TTR
CABP1
KCNF1
DDIT4L
UCN3
DGAT2
SDC4
SULT2B1
GCK
log2(FC)
Control
WY14643
G
Immature β Cell
EHF
HMGB2
PTN
ITGB4
CAPN6
EPHB3
CD9
ELN
BARX2
CLDN10
SOSTDC1
EVPL
EMP1
KRT23
MEOX1
PNLIPRP1
KRT80
SPARCL1
CCKAR
CXCL10
log2(FC)
Control
WY14643
H
OXPHOS
log2(FC)
Control
WY14643
I
Glucose Transporters and Glycolytic Enzymes
ALDOA
BPGM
ENO1
ENO2
GAPDH
GCK
GLUT1
GLUT2
GLUT3
GPI
HK1
HK2
HKDC1
PFKL
PFKM
PGAM1
PGAM2
PGAM4
PGK1
PKLR
PKM
TPI1
log2(FC)
Control
WY14643
J
Secreted Insulin/Total Insulin (pg/ng)
**
1.67G
16.7G
30KCl
1.67G
16.7G
30KCl
Insulin Stimulation Index (16.7G/1.67G)
Control
WY14643
K
2G
20G
Oligomycin
FCCP
KCN
p=0.057
OCR (Fractional change vs. basal)
Control
WY14643
Time (min)
L
Control
WY14643
NDUFA9
Vinculin
Densitometry (Fold Change)
*
Control
WY14643

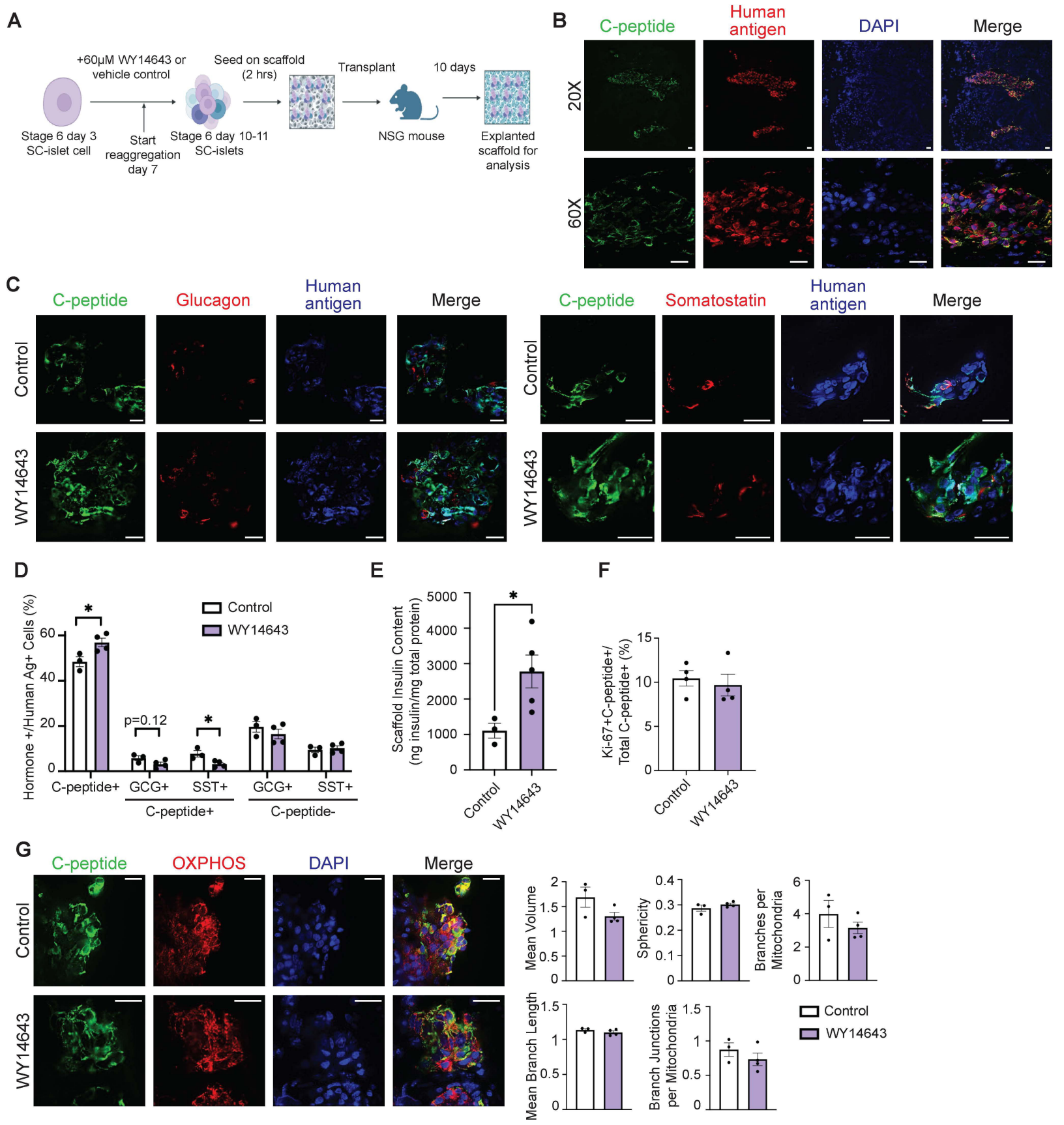
A
+60μM WY14643 or vehicle control
Seed on scaffold (2 hrs)
Transplant
10 days
Stage 6 day 3 SC-islet cell
Start reaggregation day 7
Stage 6 day 10-11 SC-islets
NSG mouse
Explanted scaffold for analysis
B
C-peptide
Human antigen
DAPI
Merge
20X
60X
C
C-peptide
Glucagon
Human antigen
Merge
Control
WY14643
C-peptide
Somatostatin
Human antigen
Merge
Control
WY14643
D
Hormone +/Human Ag+ Cells (%)
Control
WY14643
p=0.12
C-peptide+
GCG+
SST+
GCG+
SST+
C-peptide+
C-peptide-
E
Scaffold Insulin Content (ng insulin/mg total protein)
Control
WY14643
F
Ki-67+C-peptide+/ Total C-peptide+ (%)
Control
WY14643
G
C-peptide
OXPHOS
DAPI
Merge
Control
WY14643
Mean Volume
Sphericity
Branches per Mitochondria
Mean Branch Length
Branch Junctions per Mitochondria
Control
WY14643